REPORT NO. CASD-SST-73-001
CONTRACT NAS 8-26363

AEROELASTIC EFFECTS ON SPACE SHUTTLE DYNAMICS

FINAL REPORT

GENERAL DYNAMICS
Convair Aerospace Division

REPORT NO. CASD-SST-73-001

AEROELASTIC EFFECTS ON SPACE SHUTTLE DYNAMICS

FINAL REPORT

29 June 1973

Prepared Under
Contract NAS8-26363

Submitted to
National Aeronautics and Space Administration
GEORGE C. MARSHALL SPACE FLIGHT CENTER
Huntsville, Alabama

Prepared by
CONVAIR AEROSPACE DIVISION OF GENERAL DYNAMICS
San Diego, California

Page Intentionally Left Blank

FOREWORD

This report presents the third year results of an investigation conducted under Contract NAS8-26363 for NASA George C. Marshall Space Flight Center under the technical direction of the Aero-Astrodynamics Laboratory, Dynamics and Control Division. Dr. S. Winder was the technical monitor. The study was performed by Convair Aerospace Division of General Dynamics under the direction of Mr. R. Huntington, project leader. Mr. H. Riead was the principal investigator of the work reported herein and co-authored this report with Mr. Huntington.

Page Intentionally Left Blank

TABLE OF CONTENTS

LIST OF FIGURES

LIST OF FIGURES (Continued)

LIST OF TABLES

Page Intentionally Left Blank

SUMMARY

This report presents the third year results of an investigation conducted for NASA George C. Marshall Space Flight Center under Contract NAS8-26363. The first two years of the study, summarized in prior reports, dealt with the development of a computer program for the detailed analysis of the space shuttle turbulence response problem, and its application to the fully reusable shuttle concept.

The present investigation evaluates the effects of analysis simplifications on the accuracy of the results. These simplifications are made in two areas: the aerodynamic representation and the response analysis formulation. It was found that both of these shortcuts are justifiable for preliminary design studies wherein the basic data are ill defined and/or subject to change.

Applying these simplified tools to the current space shuttle configuration has revealed that the design gust loads increase the static loads at maximum αQ by approximately 50-percent.

The static aeroelastic analysis revealed that the space shuttle is a "stiff" vehicle by launch vehicle standards. Elastic effects generally increased the rigid vehicle loads by 3-percent or less.

The autopilot became unstable when the ten elastic modes were included. When only the first elastic mode was included, the system was stable.

It was also found that at the nose of the orbiter, the design gust produced a peak acceleration of 1.8g. This compares to 1.6g found in earlier analyses of the fully reusable space shuttle configuration.

SECTION 1

INTRODUCTION

This report summarizes the third and final year's work under Contract NAS8-26363, Aeroelastic Effects on Shuttle Vehicle Dynamics. References 1 and 2 present the first year's results. The second year effort is reported in Reference 3.

The first phase of the study involved the development of a computer program to determine the response of space shuttle to atmospheric turbulence. Using this program, space shuttle response characteristics were evaluated during the second study phase. Results of these investigations are summarized in Reference 4.

While this approach produced accurate results and a reliable description of the vehicle dynamic characteristics, it was time consuming and expensive due to the large amounts of data that were processed. For early design analysis, when configuration data is subject to change, this degree of sophistication is unwarranted. Accuracy may be sacrificed for quicker computer turnaround and simpler data preparation. For this reason, the study reported herein was undertaken. Specifically, the objectives were to develop a simplified analysis procedure for determining static and dynamic aeroelastic loads for space shuttle and to apply them to the current shuttle configuration.

The analysis of References 3 and 4 was based on the fully reusable space shuttle concept shown in Figure 1-1. Since that time, the shuttle has evolved into the configuration pictured in Figure 1-2, upon which the present analysis was performed.

In simplifying the turbulence response analysis approach, it was decided to modify an existing computer program developed for the Atlas launch vehicle and described in detail in Reference 5. In subsequent discussions, this is referred to as the "simplified" method. The technique of References 1-4 is called the "detailed" approach herein.

The major differences in these two methods are listed in Table 1-1. Basically, the detailed method is more general, requires more input data preparation, needs more computer core, and has a higher running time.

Section 2 of this report presents the verification of the simplifications made in the aeroelastic analyses. The simplified analysis of the present shuttle configuration is contained in Section 3. Significant conclusions of this study are given in Section 4.

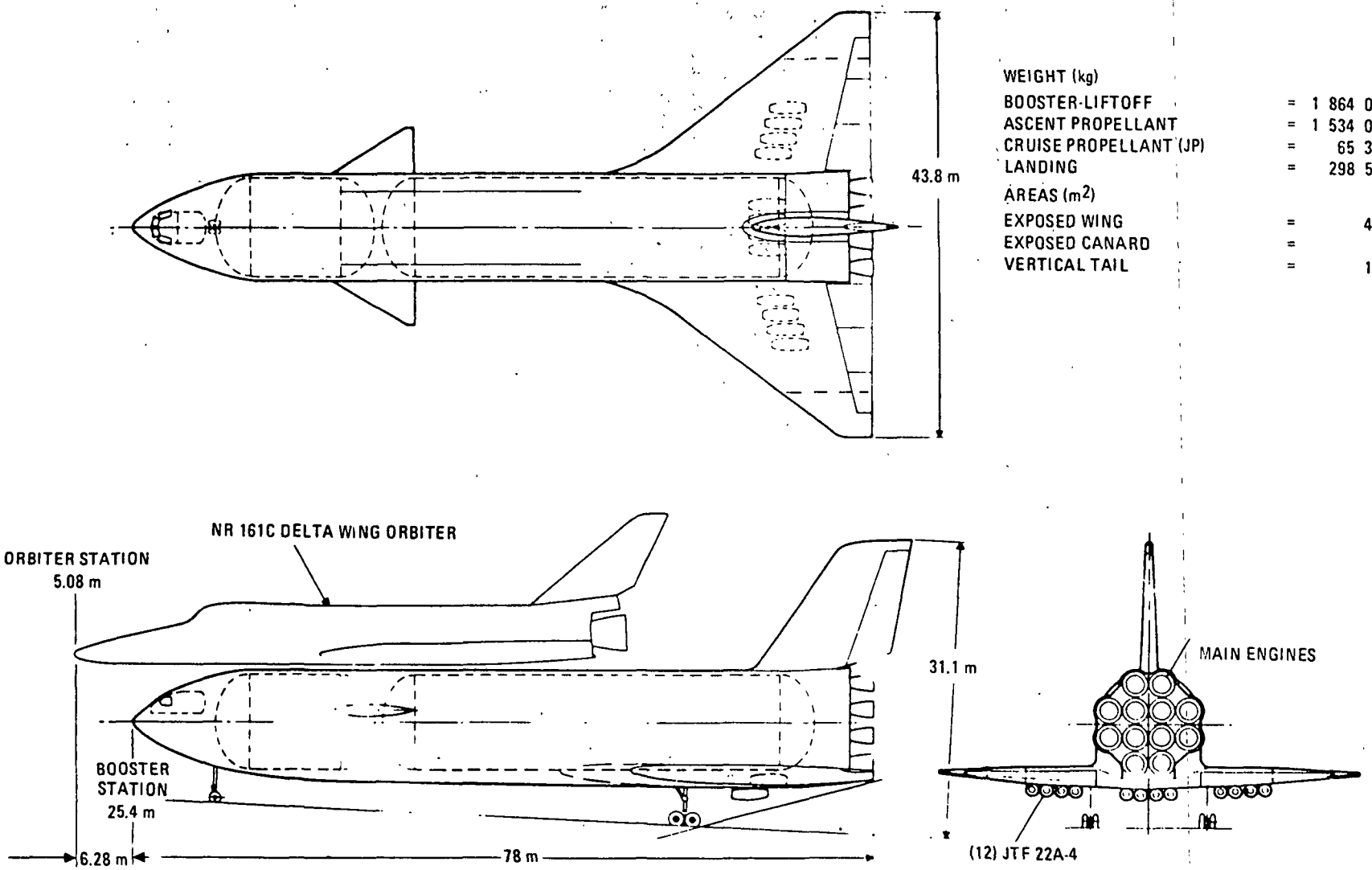

Figure 1-1. Fully Reusable Space Shuttle

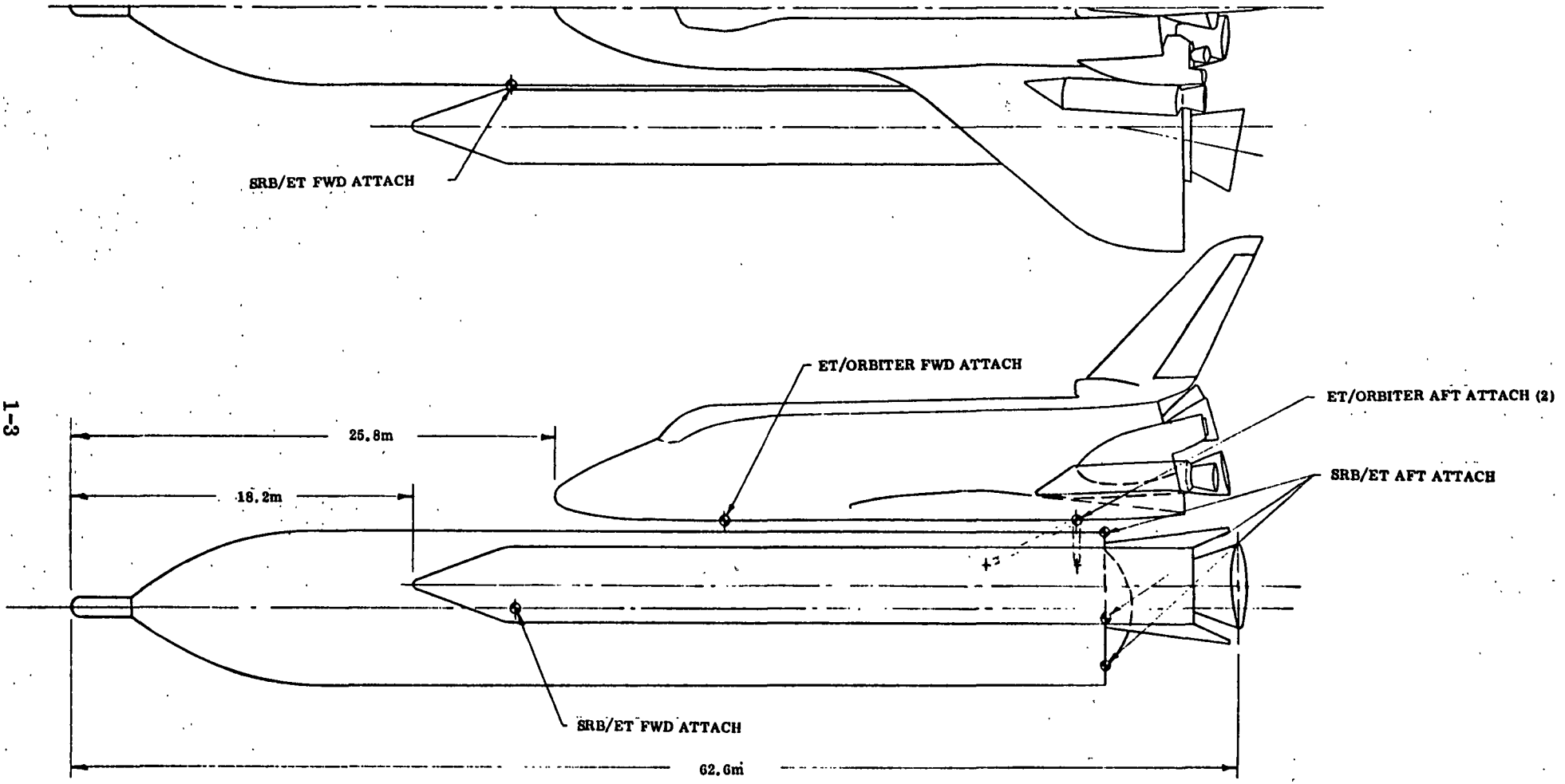

Figure 1-2 Study Vehicle

Table 1-1

Comparison of Detailed and Simplified Methods

Item	Detailed	Simplified
Analysis domain	Frequency	Time
Aerodynamics	Complex unsteady	Lumped C_{N_α}
Autopilot	General	Specific (Atlas)
Structure	General	Beam-type
Independent controls	8	1
Rigid body D.O.F.	Symmetric (2-D.O.F.) or Antisymmetric (3-D.O.F.)	Planar (2-D.O.F.)

SECTION 2

VERIFICATION OF SIMPLIFIED ANALYSIS METHOD

Prior to analyzing the configuration shown in Figure 1-2, it was necessary to evaluate the effects of the simplification on the accuracy of the results. To do this, the detailed analysis of Reference 3 was used as a yardstick.

Figure 2-1 illustrates the comparisons made. First, using the detailed analysis procedure, the effect of lumping the aerodynamic data was evaluated. Then using the lumped data the detailed and simplified turbulence response methods were compared. These evaluations are now discussed in detail.

2.1 Interference Versus Lumped Aerodynamics

The Woodward steady aerodynamic method of Reference 6 was applied to the configuration shown in Figure 1-1. Figure 2-2 illustrates the aerodynamic panel representation. The five aerodynamic surfaces are represented by 91 panels distributed on their midplanes. The bodies consist of 126 total panels. Reference 3 presents the aerodynamic analysis in detail.

In the Woodward method, the panels represent planes through which there is zero flow. For a single panel the zero flow condition is accomplished by summing the cross flow components resulting from sources representing the body shape, transient disturbances, etc. and setting a singularity strength at the panel to cancel the total flow. When there is more than one panel in the flow field, the cross flow at a given panel will be, in general, also a function of the singularity strengths of the other panels. Thus, to establish the condition of zero cross flow at all panels simultaneously, a matrix relating the cross flow at a panel to the singularity strengths at all other panels is required. This matrix is called the aerodynamic influence coefficient matrix [A].

Neglecting, for the moment, the sources, sinks and vortices also used in the Woodward solution, the change in the pressure difference across the panels $\{\Delta p\}$ resulting from a change in the cross flow distribution at the panels $\{\Delta n\}$ caused by a transient disturbance is given by the simple relationship

$$\{\Delta p\} = [A]^{-1} \{\Delta n\} \qquad (1)$$

Equation (1) might be expected to give poor results in the vicinity of the noses of the bodies since the aerodynamic panels do not represent the nose shapes. The actual body shapes are represented by extending a series of sources and doublets along the body center lines. The source strengths, a function of body geometry and Mach number only are not affected by a transient disturbance and therefore do not enter into the gust response solution. The doublet strength at a point in a body is a function of the cross flow at that point.

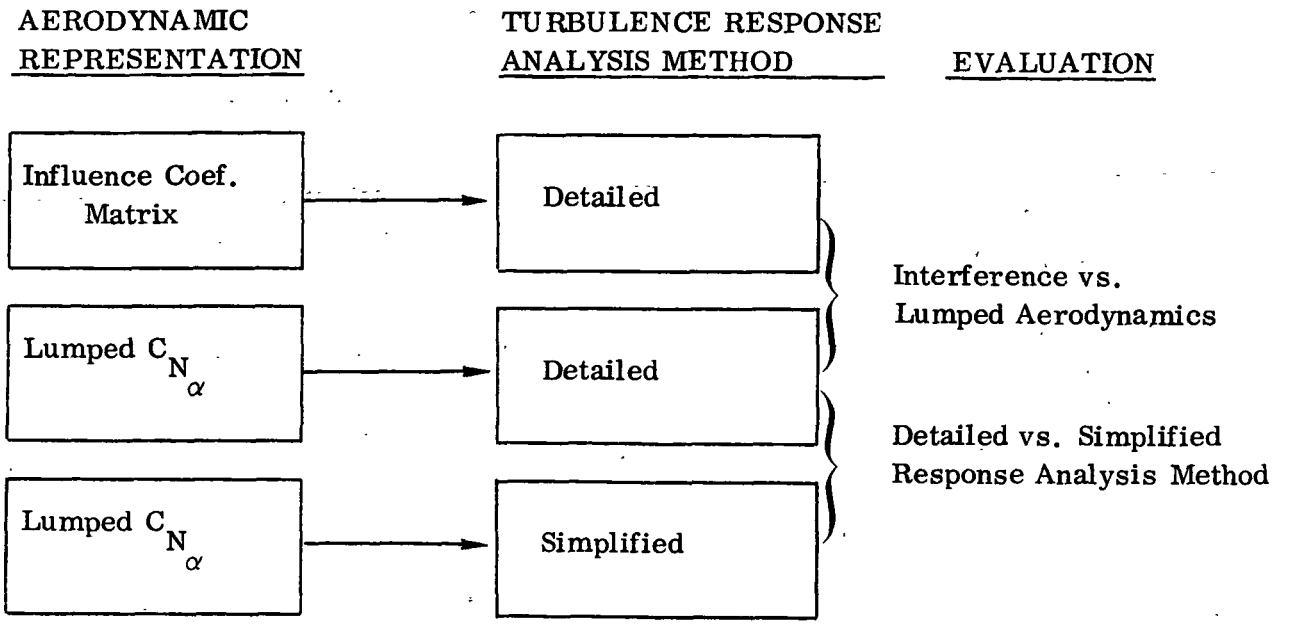

Figure 2-1. Method Verification Approach

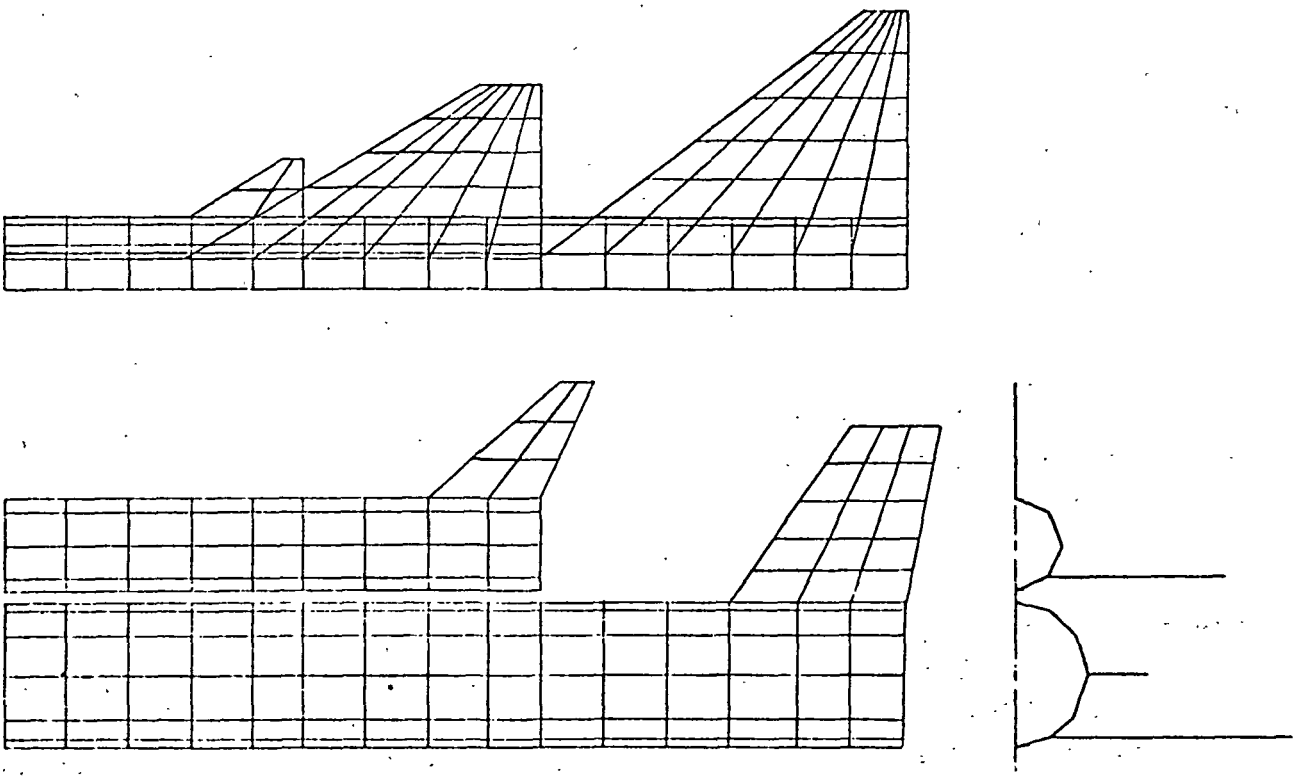

Figure 2-2. Aerodynamic Panel Representation

Since both gusts and vehicle response produce cross flow along the body these doublet strengths must be included in the gust response solution. In subsequent discussions the body doublets are included in [A].

Computation of generalized forces from large aerodynamic influence coefficient matrices is an expensive and time consuming process. Furthermore, the response problem formulation is simplified if the aerodynamics are expressed in terms of local lift curve slopes lumped at structural node points on the vehicle. For these reasons, a simple approach which involves replacing the influence coefficient matrix with an "equivalent" diagonal matrix is suggested. For any steady-state vehicle angle of attack, this method gives the "exact" total lift and pressure distribution. Specifically, equation (1) can be rewritten

$$\frac{1}{Q}\{\Delta p\} = \left[C_{N_\alpha}\right]\{\alpha_s\} = V[A]^{-1}\{\alpha_s\} \tag{2}$$

where Q is dynamic pressure, $\{\alpha_s\}$ is the steady state angle of attack distribution, V is velocity, and

$$C_{N_{\alpha_{ii}}} = \frac{V}{\alpha_i}\left(a_{i1}\alpha_1 + a_{i2}\alpha_2 + \ldots\ldots a_{im}\alpha_m\right) \tag{3}$$

where a_{ij} is an element of $[A]^{-1}$ and m is the total number of aerodynamic panel points.

To evaluate the effect of lumping the aerodynamics, symmetric responses at Mach 1.2 were calculated. Figure 2-3 shows booster wing root shear magnitude as a function of gust frequency. A unit amplitude sinusoidal gust was assumed. The shear magnitude was normalized to the value obtained for a zero frequency (infinite wavelength) gust. The shear is that resulting from the gust only and does not include shear due to vehicle response. It can be seen that while the results produced by the two methods are similar for long wavelength gusts, there is a considerable difference for gusts of shorter wavelength. This difference is primarily attributable to downwash produced on the booster wing by the orbiter wing as is indicated by the approximate solution, obtained by holding the downwash on all bodies and surfaces, other than the booster and orbiter wings, constant at the values obtained for $\omega = 0$.

The normalized transfer function magnitudes, giving total vehicle lift resulting from a unit sinusoidal gust, are shown in Figure 2-4, as a function of gust frequency. Differences between the interference aerodynamics and lumped aerodynamics transfer functions are less pronounced in this case than for booster wing root shear, but discrepancies still exist for shorter wavelength gusts.

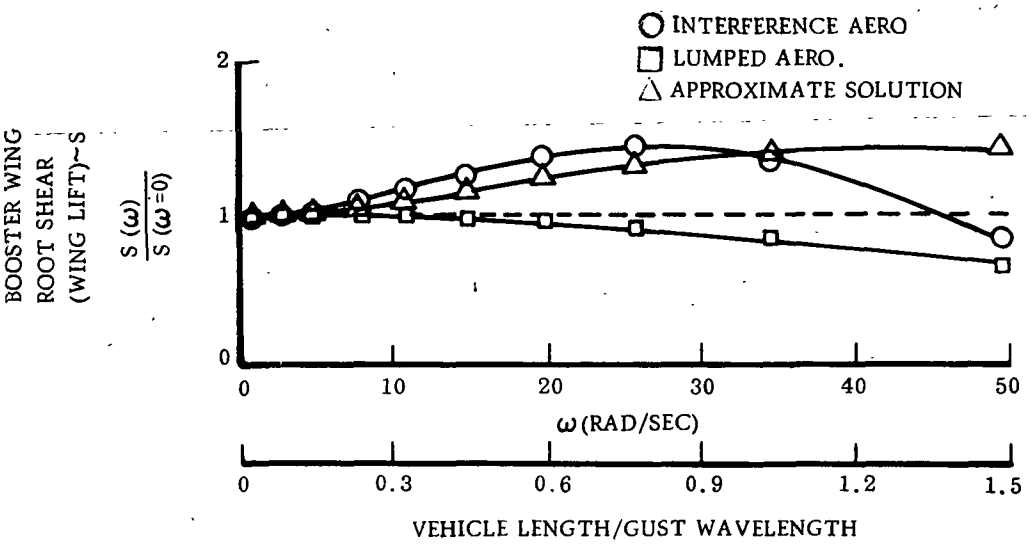

Figure 2-3. Booster Wing Root Shear Transfer Functions

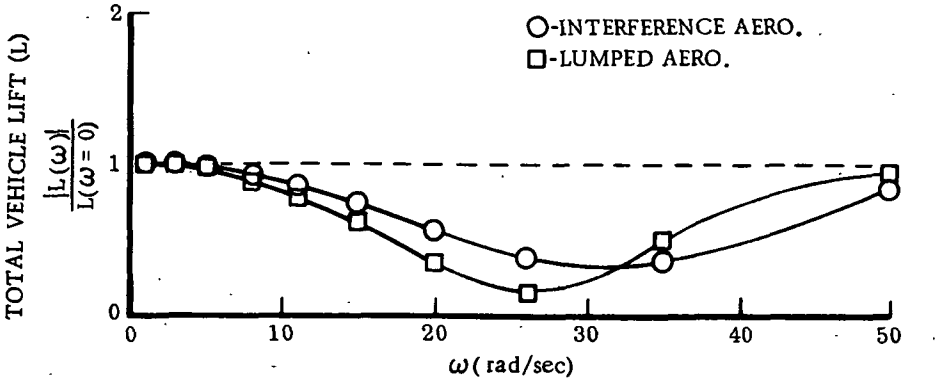

Figure 2-4. Total Vehicle Lift Transfer Functions

To determine if a significant amount of energy could be expected to be concentrated in the shorter wavelength gusts where the differences between the two methods are appreciable, the 99th percentile power spectrum from Reference 7 was used. This spectrum is shown in Figure 2-5.

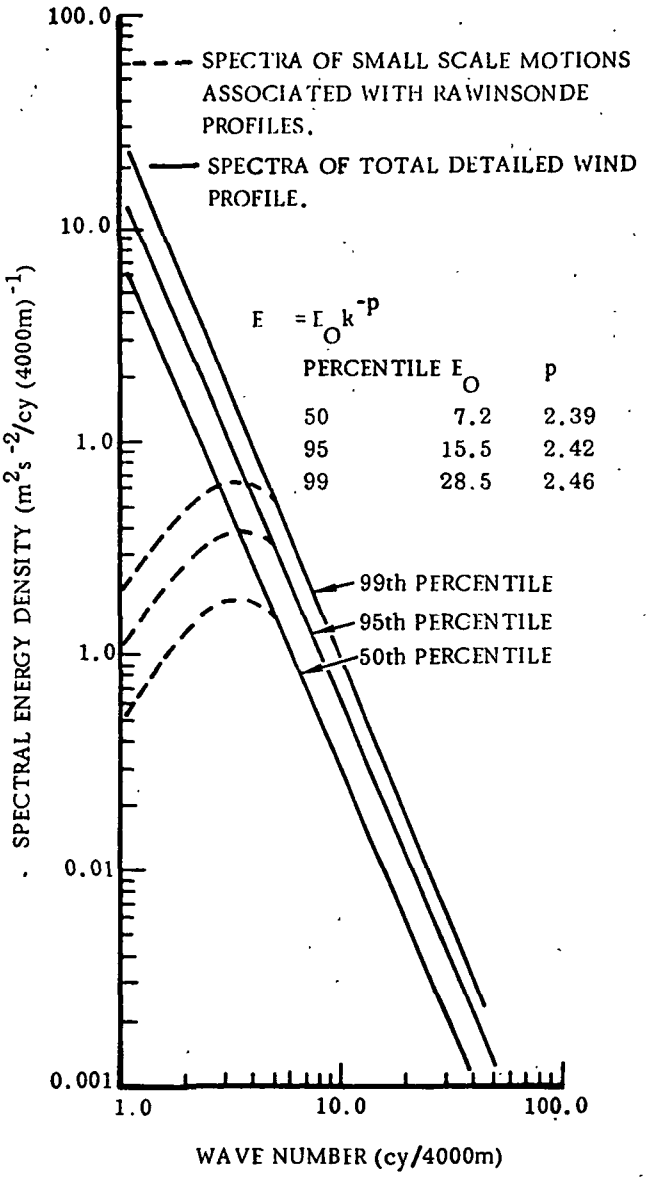

Figure 2-5. Spectra of Detailed Wind Profiles (Reference 7)

The root-mean-square (RMS) booster wing root shear and RMS vehicle lift resulting from this spectrum are shown in Figures 2-6 and 2-7. The quantities

$$\int_0^{\omega_c} E(\omega)\, S^2(\omega)\, d\omega \qquad \text{and} \qquad \int_0^{\omega_c} E(\omega)\, L^2(\omega)\, d\omega \tag{4}$$

are the RMS booster wing root shear and RMS vehicle lift, respectively, resulting from all gust frequencies $\omega \leq \omega_c$. The curves were normalized by dividing by the interference aerodynamics RMS values at $\omega_c = 50$. These curves indicate that most of the power in the gust spectrum is concentrated at low frequencies where the differences between the two methods are slight.

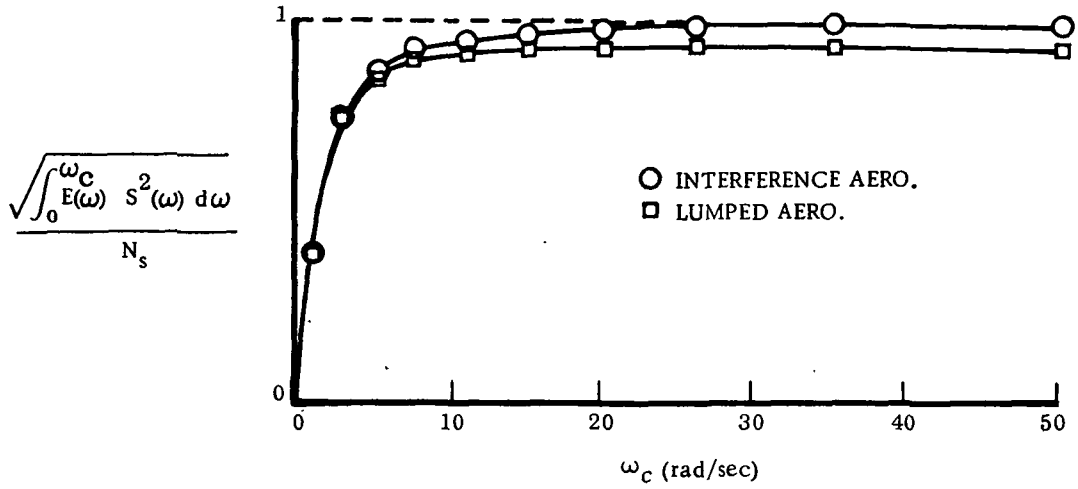

Figure 2-6. Booster Wing Root Shear RMS Response

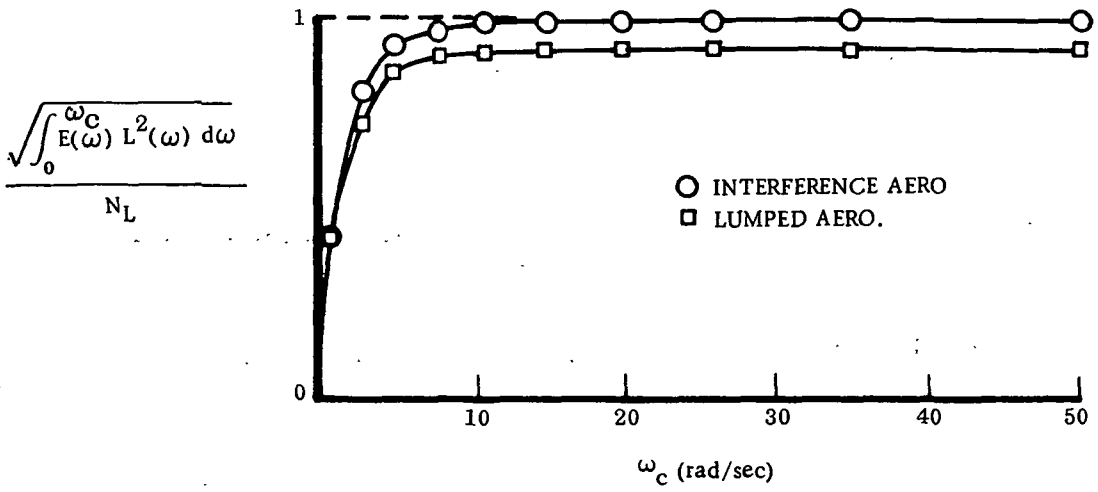

Figure 2-7. Vehicle Lift RMS Response

To determine the effect of interference on vehicle response to a discrete gust, the quasi-square wave gust from Reference 7 was used. This gust and its Fourier series representation used in the response analysis are shown in Figure 2-8. The gust wavelength was "tuned" to excite the lowest vehicle elastic modes.

The response time histories of booster wing root shear and booster center of gravity acceleration resulting from this discrete gust are shown in Figures 2-9 and 2-10. Time histories are shown for vehicle plunge only (1 degree of freedom), vehicle plunge and pitch (rigid body) and for a full elastic representation including the two vehicle rigid body modes, eight elastic modes and booster LO_2 and LH_2 slosh. The interference aerodynamics solution is indicated by the solid line and the lumped aerodynamics solution is indicated by the dashed line. It can be seen that the agreement is generally good.

Based on the random and discrete gust analysis results presented above, it can be concluded that the simplification in going from interference to lumped aerodynamic data is justifiable for preliminary design analysis.

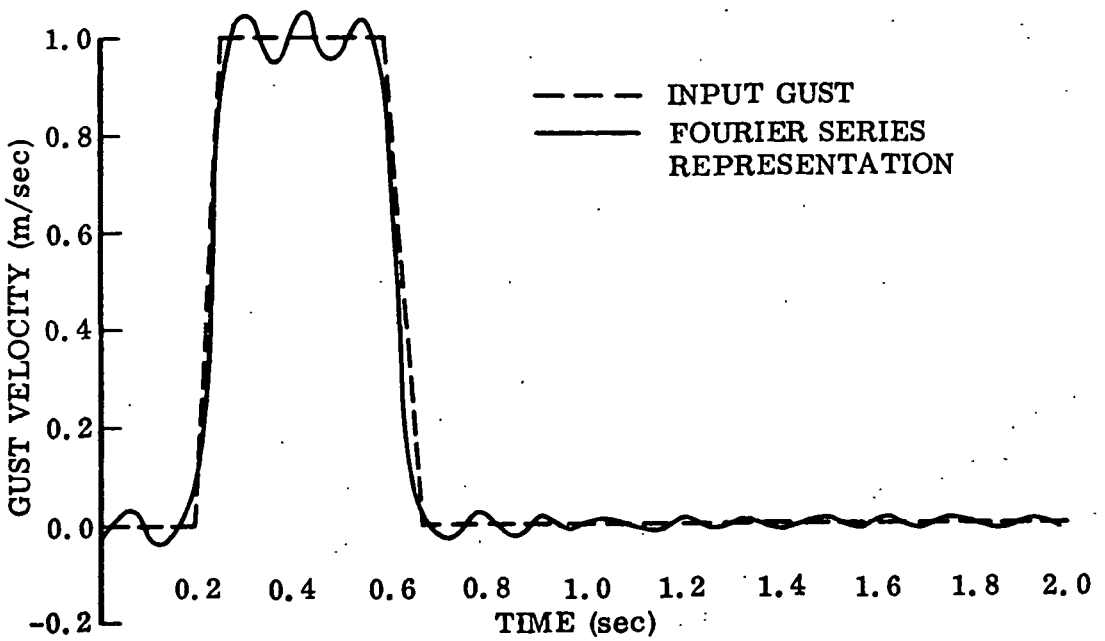

Figure 2-8. Discrete Gust Time History

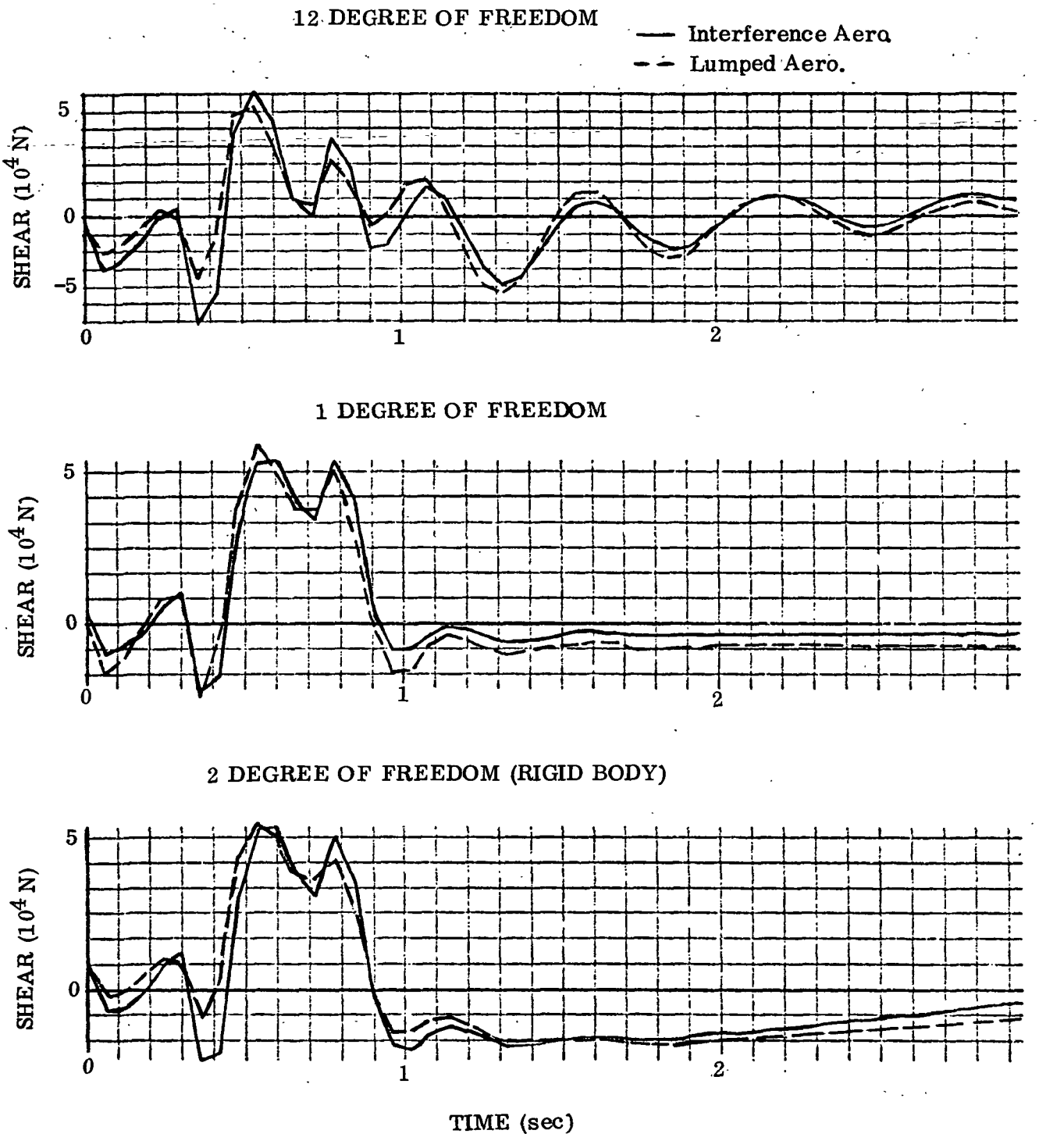

Figure 2-9. Booster Wing Root Shear Response to 1 m/sec. Quasi-Square Gust.

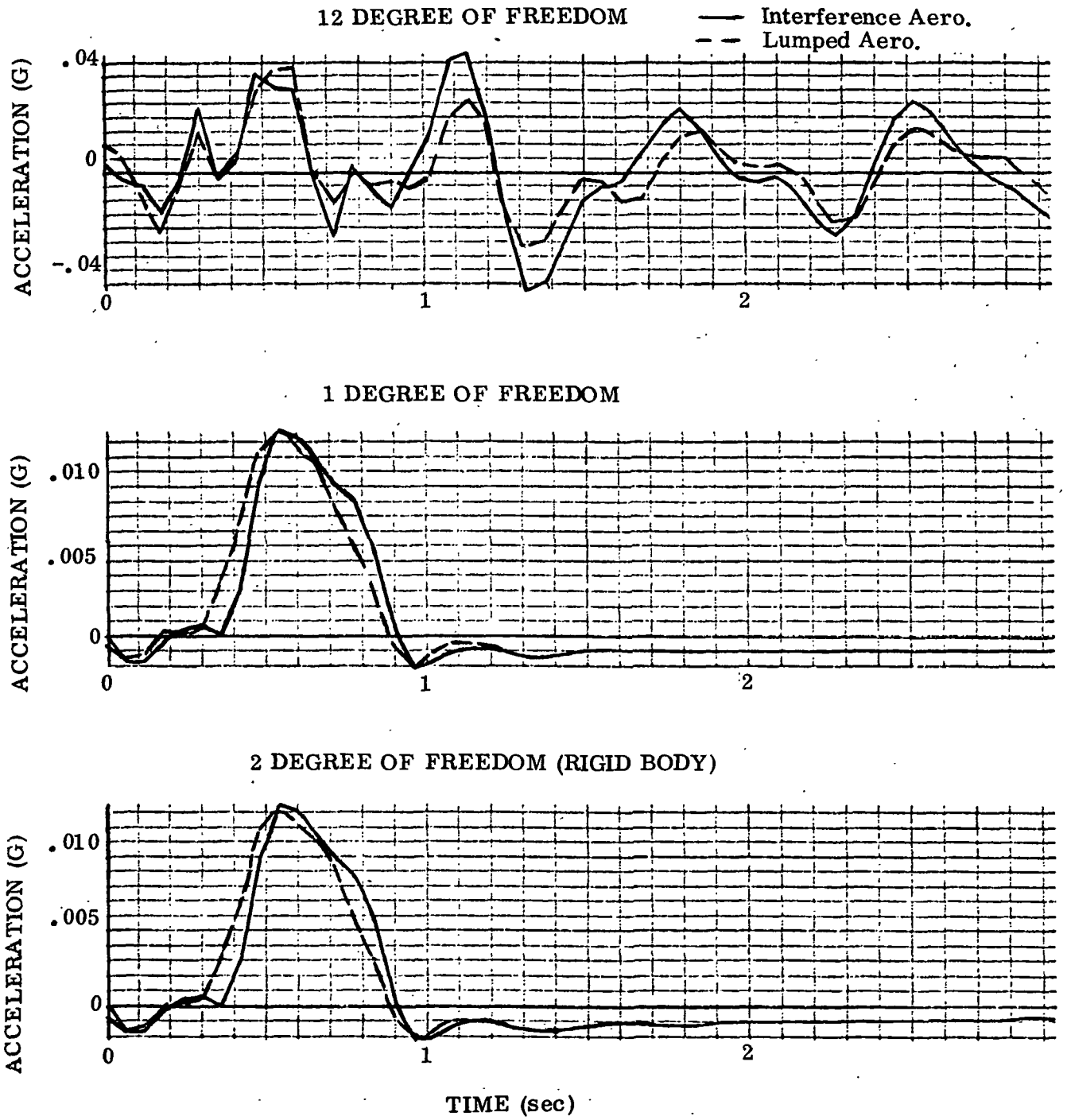

Figure 2-10. Booster Center of Gravity Acceleration Response to 1 m/sec. Quasi-Square Gust.

2.2 Detailed Versus Simplified Turbulence Response Analysis Method

A comparison of the detailed and simplified gust analysis methods was made at Mach 1.2. Since the simplified analysis is a time domain formulation, the discrete gust shown in Figure 2-8 was assumed. The gust was represented by the straight (dashed) line segments as opposed to the Fourier series approximation used in the detailed analysis.

Results are shown in Figure 2-11 in terms of booster body acceleration time histories at stations 29.2m and 99.4m. Figure 2-12 shows the corresponding booster wing tip acceleration responses obtained by the two methods. Although the shapes of the response curves obtained by the two methods are somewhat different, their trends are similar and their peak amplitudes are nearly the same. The initial response in the detailed analysis results from the oscillations in the Fourier gust representation shown in Figure 2-8. From this standpoint, the simplified analysis yields more accurate results.

These evaluations indicate that for preliminary design studies, where basic data are generally subject to change, the simplified analysis method yields acceptable results.

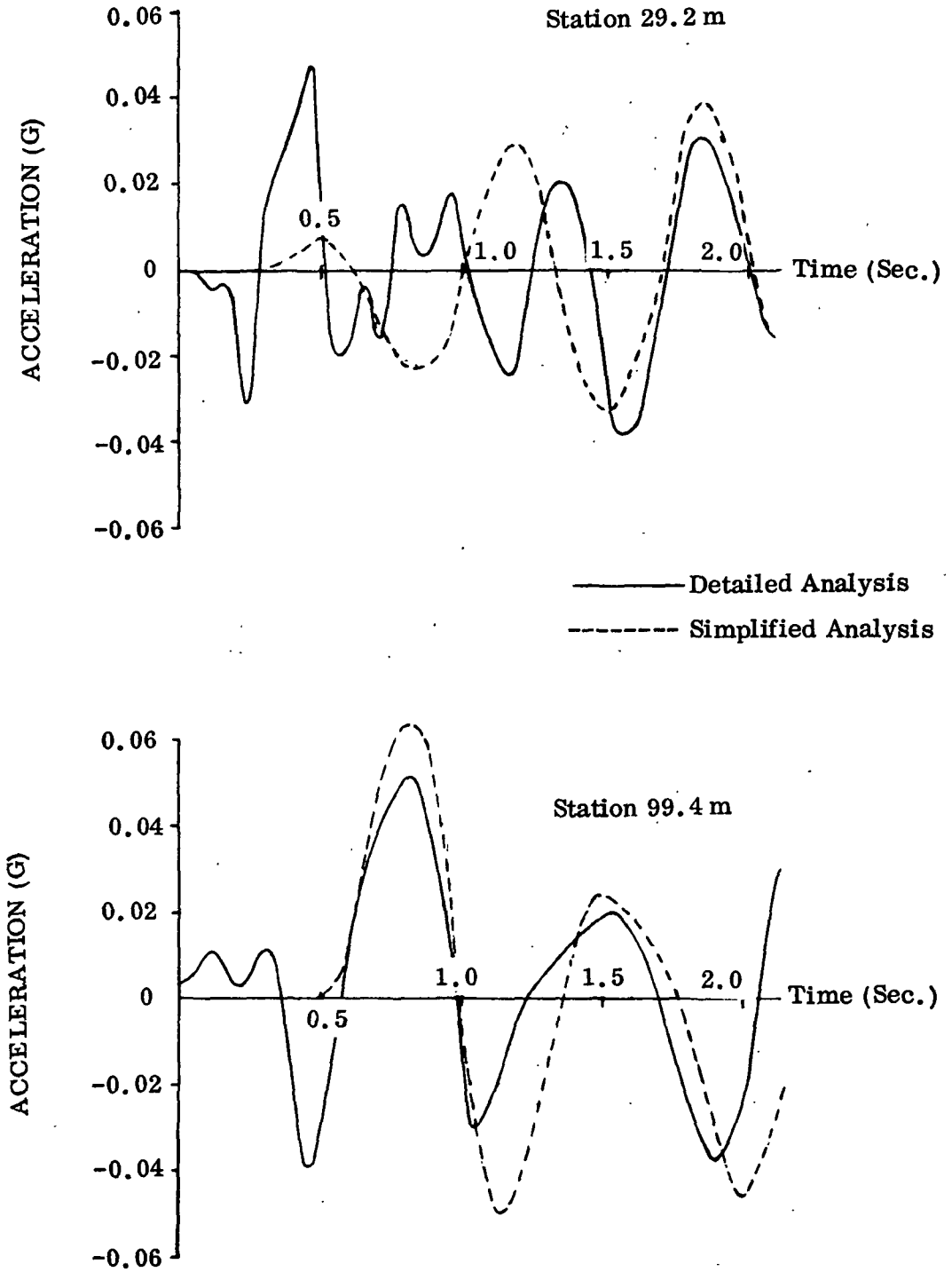

Figure 2-11. Booster Body Accleration Response to 1-m/s Quasi-Square Wave Gust

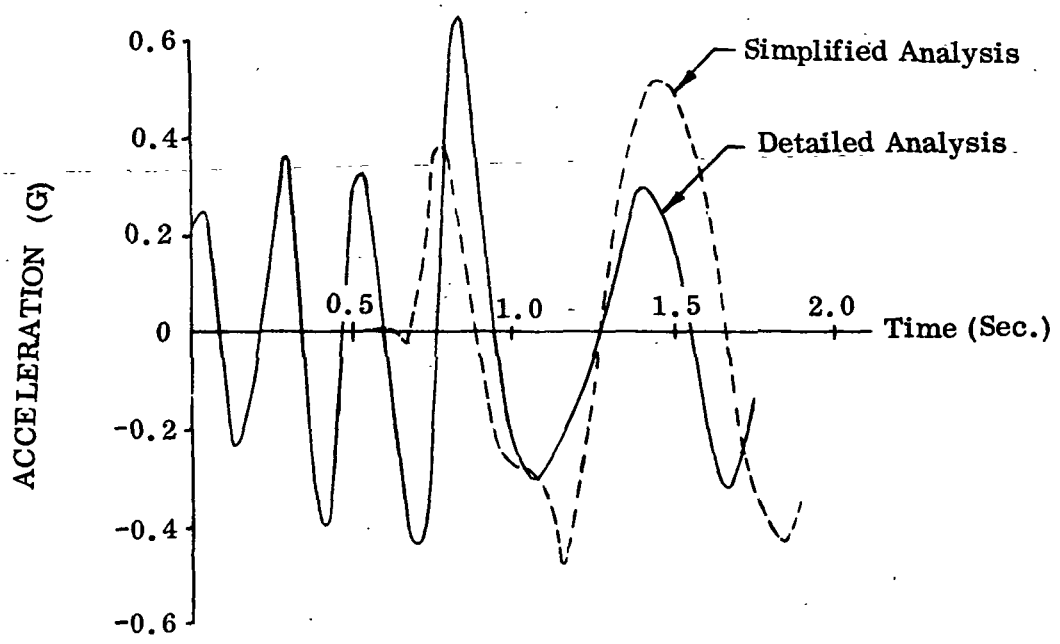

Figure 2-12. Booster Wing Tip Accleration Response to 1-m/s Quasi-Square Wave Gust

SECTION 3

SIMPLIFIED AEROELASTIC ANALYSIS

The configuration shown in Figure 1-2 was analyzed during ascent flight at Mach numbers 0.8 and 1.2. Two types of analysis were performed: static aeroelastic loads determination and gust response.

Basic data defining the configuration were provided by MSFC in the form of vibration modes, aerodynamic derivatives, autopilot parameters and trajectory information.

The vehicle analyzed is not the "latest" space shuttle configuration, but represents the general characteristics of the present concept. The results, therefore, are intended to reflect trends and gross aeroelastic behavior of the shuttle during maximum dynamic pressure ascent flight.

3.1 Static Aeroelasticity

The static aeroelastic analysis was performed using the computer program described in Reference 8. The procedure is one in which the vehicle is represented by its structural flexibility matrix. Lumped masses, aerodynamic normal force coefficient derivatives, C_{N_α}, and zero angle of attack coefficients, C_{N_0}, are distributed at "nodes" on the structural model. The vehicle is assumed to be trimmed against a specified value of angle of attack, α, and dynamic pressure, Q, by vectoring the engine thrust. Due to the resulting net force, the vehicle accelerates, producing distributed inertia forces. The combination of aerodynamic thrust and inertia forces act on the flexibility matrix to distort the vehicle, causing a change in the external loads. After several iterations, the process converges to acceptable limits.

Prior to the static aeroelastic analysis, a 47-node beam-type structural model was formed to generate the required flexibility matrix. The model is shown in Figure 3-1. Table 3-1 lists the masses and lumped aerodynamic data. For simplicity, the mass data was held constant at the two Mach numbers. The values listed represent half of the vehicle. The reference area upon which the aerodynamic data are based is 300 m^2. Total values for half the vehicle are listed in Table 3-2. Stiffnesses for the external tank (ET) and solid rocket booster (SRB) were provided by MSFC. Orbiter stiffnesses were scaled down from those of the larger orbiter analyzed in References 3 and 4. The orbiter/ET and ET/SRB attachment stiffnesses were established by trial and error so that the lowest mode shapes and frequencies would agree as closely as possible with the modal data provided by MSFC for the gust response analysis. This was required because the flexibility matrix from which the MSFC modes were derived was unavailable.

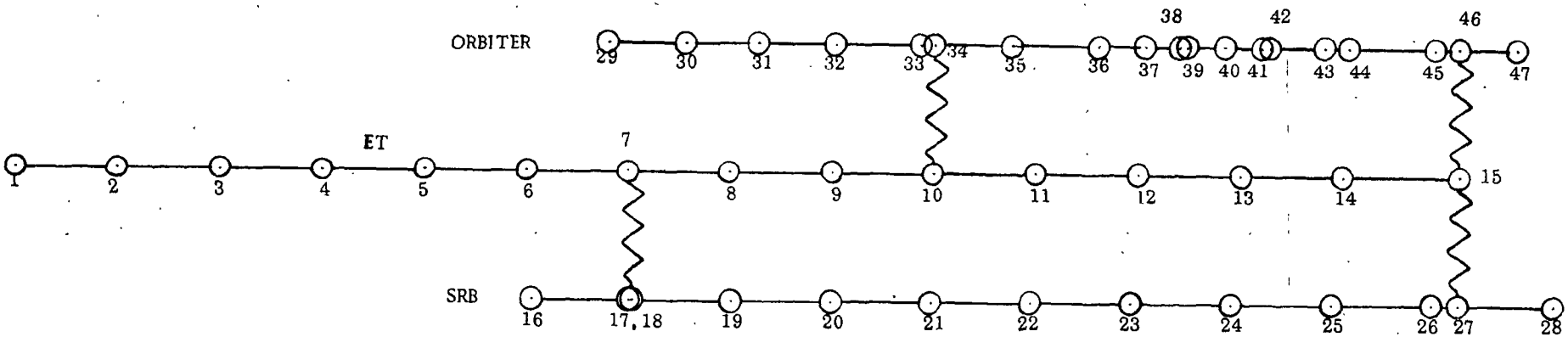

Figure 3-1. Beam-Type Structural Model

Table 3-1. Beam-Type Structural Model Mass and Aerodynamic Data

Node	Station (m)	Mass (kg)	M = 0.8		M = 1.2	
			$10^5 C_{N_\alpha}$ (deg^{-1})	$10^5 C_{N_o}$	$10^5 C_{N_\alpha}$ (deg^{-1})	$10^5 C_{N_o}$
1	2.02	3502	14.5	2.5	18.0	-7.0
2	6.06	3502	80.5	21.5	72.0	-11.0
3	10.10	3502	131.0	-10.5	233.0	-118.0
4	14.14	83916	-26.5	-43.0	168.5	-418.0
5	18.17	140162	5.0	-64.0	69.5	-107.0
6	22.21	70308	121.0	-201.5	-13.5	321.0
7	26.25	3502	212.5	-488.0	-3.5	329.5
8	30.29	7031	198.5	-501.0	-19.0	289.5
9	34.33	7031	88.0	-246.5	185.0	-1079.0
10	38.37	7031	-67.0	-139.5	190.0	-693.5
11	42.41	10524	-50.5	-117.5	24.0	-591.0
12	46.44	7031	-56.5	-54.0	-77.0	-32.5
13	50.48	7031	-62.5	137.0	-118.0	449.0
14	54.52	7031	-13.5	-11.0	-32.5	-235.5
15	59.13	7031	-10.5	348.5	-7.0	582.5
16	22.42	5262	31.0	-103.0	-12.0	21.0
17	26.25	175	0.	0.	0.	0.
18	26.38	5262	136.0	-95.0	-12.0	103.0
19	30.34	7031	62.0	-144.0	120.0	144.0
20	34.30	25810	107.0	-82.0	223.0	-227.0
21	38.27	25810	5.0	-103.0	128.0	-507.0
22	42.23	25810	10.0	-268.0	-4.0	-445.0
23	46.19	25810	33.0	-528.0	-41.0	-552.0
24	50.15	25810	58.0	-796.0	8.0	-745.0
25	54.11	25810	16.0	-350.0	-45.0	-433.0
26	58.08	25810	-41.0	1443.0	-132.0	198.0
27	59.13	175	0.	0.	0.	0.
28	62.87	54432	33.0	82.0	-37.0	664.0
29	25.45	350	15.0	0.	125.0	0.
30	28.52	350	40.0	0.	-20.0	0.
31	31.39	350	35.0	0.	40.0	0.
32	34.44	2581	15.0	0.	50.0	0.
33	37.85	3502	-10.0	0.	20.0	0.
34	38.36	175	0.	0.	0.	0.
35	41.45	3502	35.0	0.	-145.0	0.
36	44.88	5171	15.0	0.	40.0	0.
37	46.74	175	335.0	0.	340.0	0.
38	48.08	175	-50.0	0.	45.0	0.
39	48.39	0	330.0	0.	350.0	0.
40	49.83	0	310.0	0.	390.0	0.
41	51.33	1225	45.0	0.	50.0	0.
42	51.64	175	270.0	0.	350.0	0.
43	53.80	175	190.0	0.	420.0	0.
44	54.74	2277	35.0	0.	45.0	0.
45	58.14	3329	20.0	0.	130.0	0.
46	59.13	175	0.	0.	0.	0.
47	61.39	3502	20.0	0.	70.0	0.

Table 3-2. Half-Vehicle Mass and Aerodynamic Totals

Mach. No.	Mass (kg)	C. G. Station (m)	C_{N_α} (deg^{-1})	C_{N_o}	Aero. Center (m)
0.8	0.65×10^6	33.4	0.0268	-0.0203	38.7
1.2	0.65×10^6	33.4	0.0319	-0.0310	39.0

Table 3-3 compares the lowest frequencies obtained using the beam-type model with those supplied by MSFC and used in the gust response analysis reported in Section 3.2.

Table 3-3. Symmetric Mode Frequency Comparison, Beam-Type Structure Versus MSFC Modes

Mode	Frequency (H_z)	
	MSFC	Beam-Type
1	2.22	2.32
2	3.00	2.78
3	3.19	3.50*
4	3.25	
5	3.61	
6	4.19	
7	4.68	
8	4.73	
9	5.04	
10	5.40	

*The mode shape corresponds to the fourth MSFC mode.

The lowest mode shapes agree fairly well also. The first mode involves primarily orbiter pitching about its aft attach point. The second mode consists mainly of the orbiter pitching about the midpoint between its two attach points. The maximum deflection of both modes occurs at the orbiter nose.

For the static aeroelastic analysis, a product angle of attack (α) times dynamic pressure (Q) equal to 120,000 deg-N/m^2 was assumed at both Mach numbers. The dynamic pressures were 18,200 N/m^2 and 22,500 N/m^2 at Mach 0.8 and 1.2, respectively.

Results of the static aeroelastic analysis in the form of shear and bending moment distributions for the individual stages are given in Figures 3-2 through 3-4. The aft end shears and moments are not shown because the integration method used did not properly account for the shear transfer between stages at their aft attachment. The

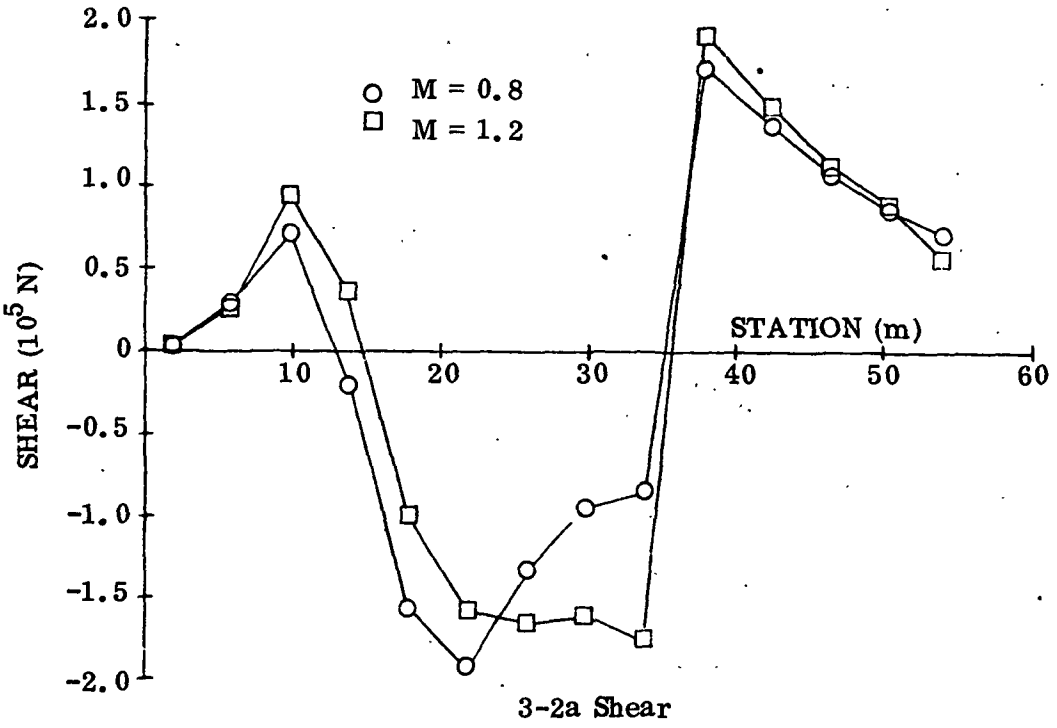

3-2a Shear

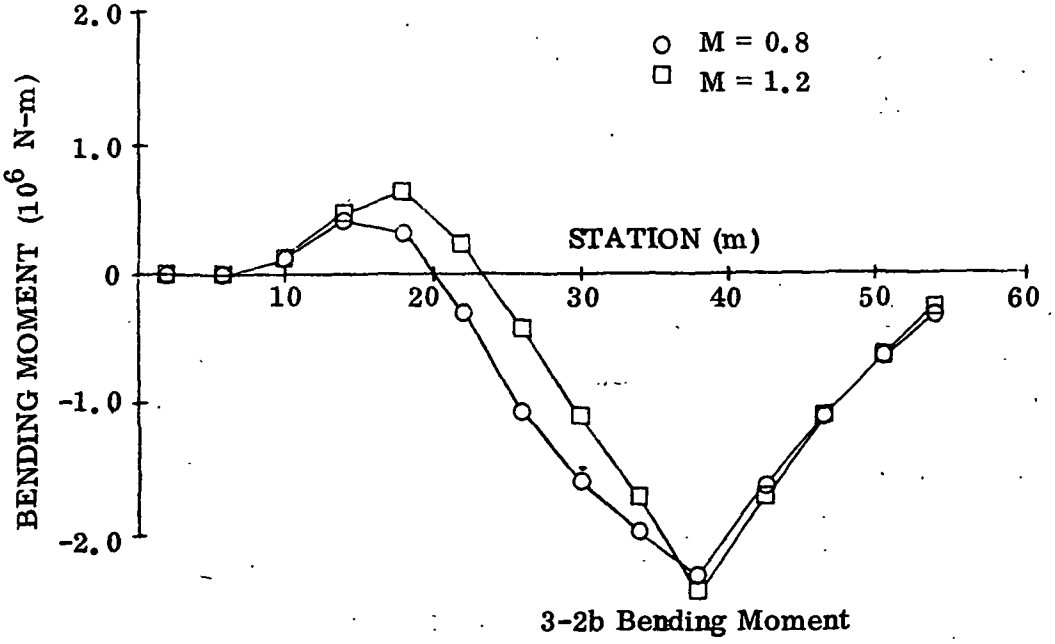

3-2b Bending Moment

Figure 3-2. ET Static Aeroelastic Load Distributions ($\alpha Q = 120000$ deg-N/m^2)

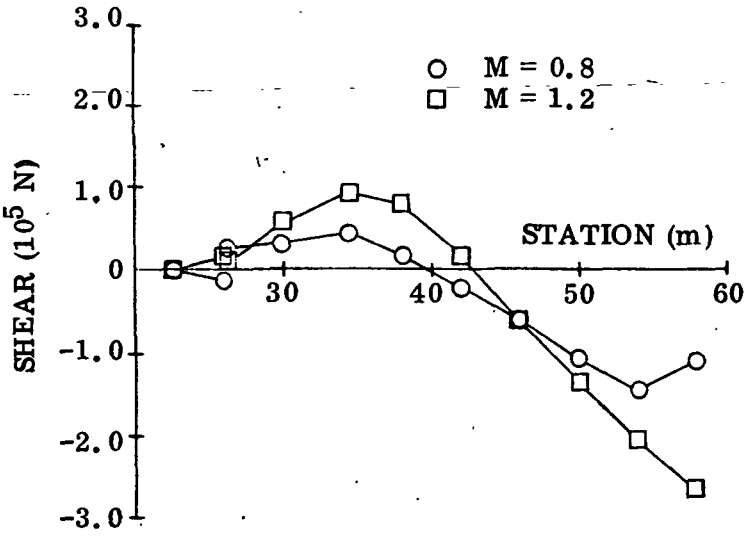

3-3a Shear

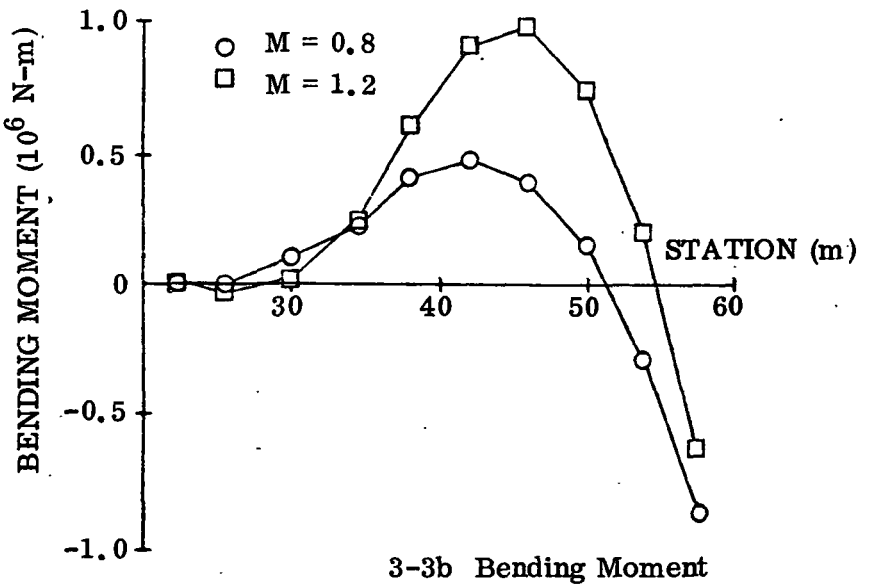

3-3b Bending Moment

Figure 3-3. SRB Static Aeroelastic Load Distributions
($\alpha Q = 120000$ deg-N/m^2)

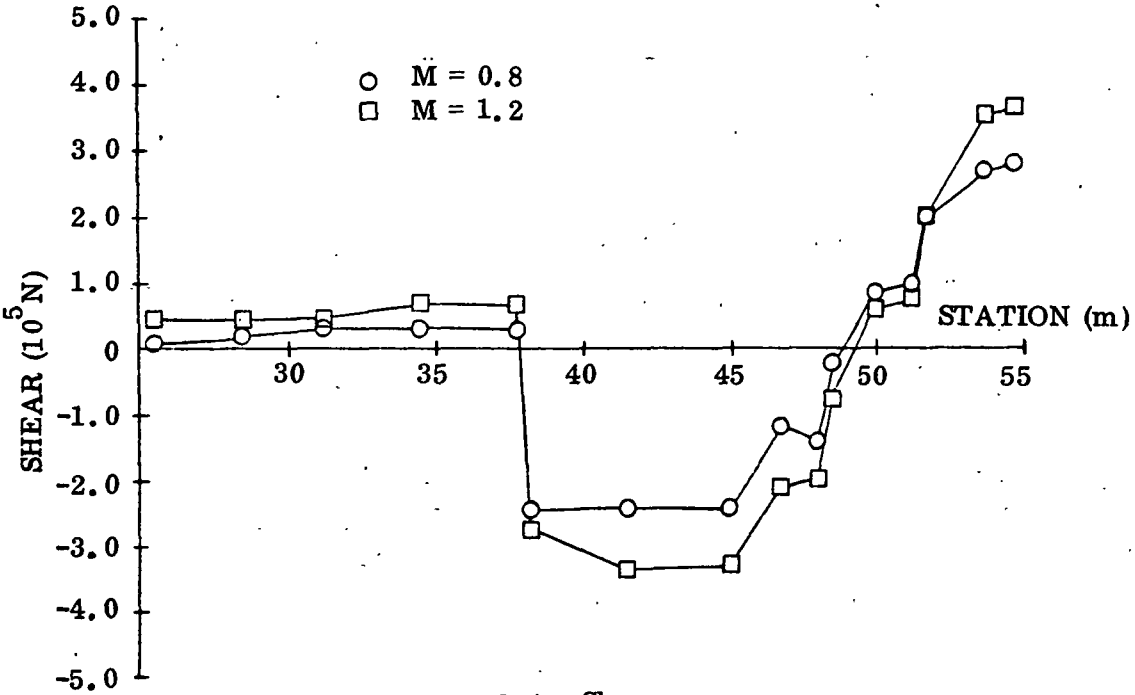

3-4a Shear

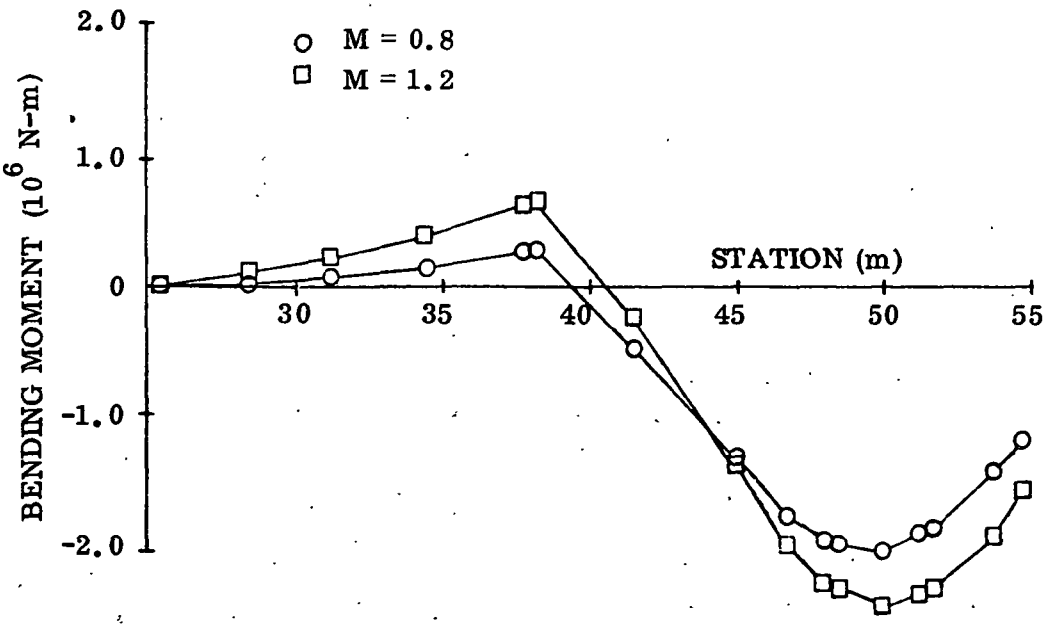

3-4b Bending Moment

Figure 3-4. Orbiter Static Aeroelastic Load Distributions (αQ = 120000 deg-N/m^2)

significant finding of this analysis is that the elastic contribution to the total shear and moment distribution is negligible. Typically, elastic deformations changed the rigid loads by less than three per cent.

3.2 Gust Response

The simplified gust response method applied in the present investigation is described in detail in Reference 5. Two additions were made to the program for this study. The program was modified to account for penetration gusts in which the gust velocity varies over the vehicle length, and the capability was added for including an additional thrust-vectored engine.

In this computer program, simultaneous second order differential equations are solved as a function of time. Generalized coordinates in the formulation include: elastic modes, rigid body modes, propellant sloshing (ignored in the present study), engine vectoring, and autopilot-sensed parameters.

As in the static aeroelastic analysis of Section 3.1, the vehicle was analyzed in the pitch plane during ascent flight at Mach numbers 0.8 and 1.2. A 1-m/s quasi-square wave gust (Figure 2-8) was assumed as the disturbance. Three gust lengths were investigated, one with its period set equal to one-half the first mode period (0.22 sec.), and the other two set at 0.11 and 0.44 seconds.

Ten elastic modes were included in the analysis. Supplied by MSFC, their frequencies are given in Table 3-3.

The autopilot, provided by MSFC, is shown in Figure 3-5. It consists of displacement rate and acceleration feedbacks driving the SRB and orbiter engines. All sensors were assumed to be located on the orbiter fuselage at station 33.4m (the combined vehicle C.G. station).

When the autopilot was used with the rigid body, plus first elastic mode, the system was stable as seen in Figure 3-6a. This figures gives the acceleration at orbiter station 38.4m as a function of time due to penetrating the 0.22-second period gust. Results are shown with and without the autopilot. Figure 3-6b shows the unstable response when all ten elastic modes are included with the autopilot. Due to this instability, the autopilot was not included in the subsequent analyses.

Figure 3-7 shows acceleration time-histories at Mach 0.8 and 1.2 due to the 0.22-second period gust. The responses are shown for each vehicle near the combined vehicle C.G. (approximately station 33.4m). These are shown to give an idea of the typical response shapes.

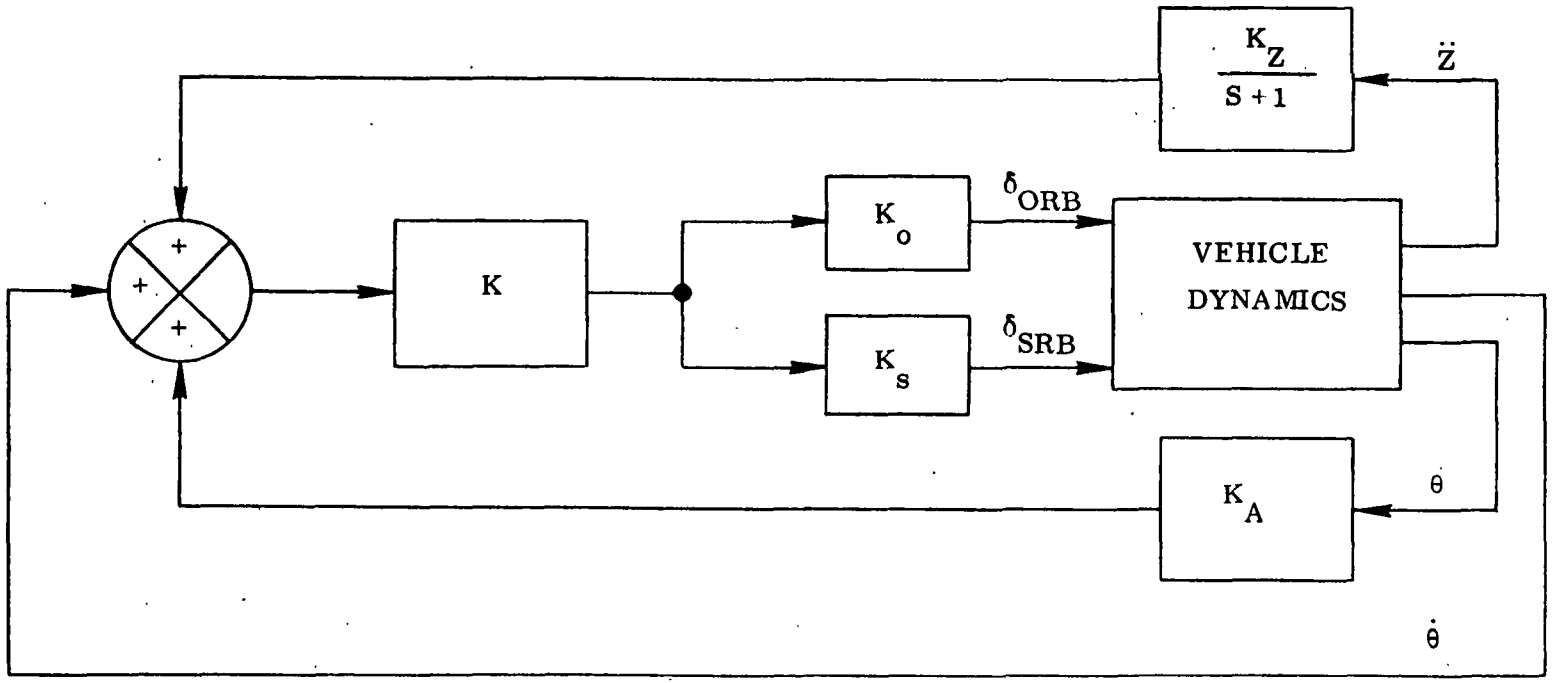

$K_Z = 0.28$ rad/sec/m/sec^2

$K_A = 0.7$ rad/sec/rad

$K = 1.1$ rad/rad/sec

$K_o = 1.4$

$K_s = 1.4$

Figure 3-5. Pitch Plane Autopilot Block Diagram

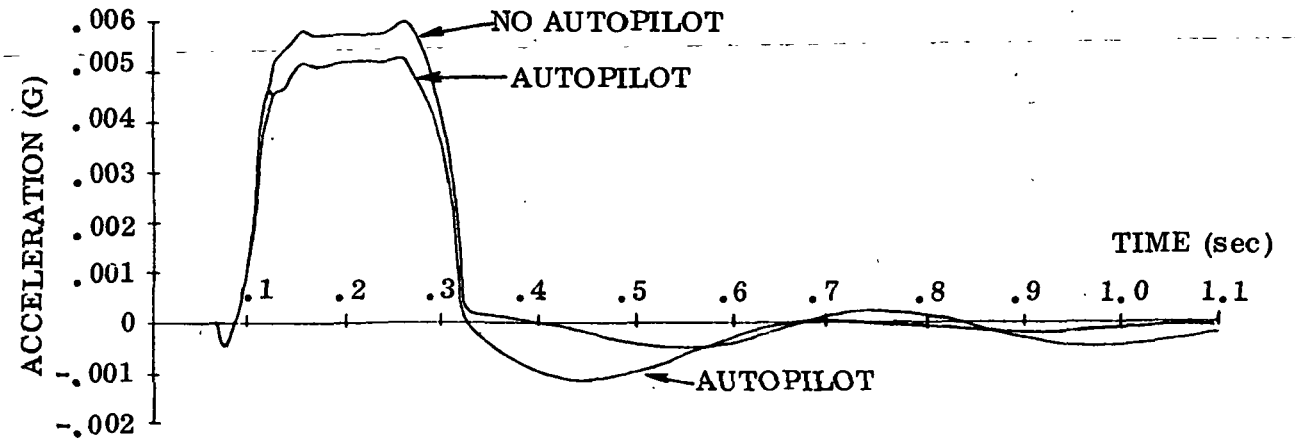

a. Rigid Body Plus First Elastic Mode

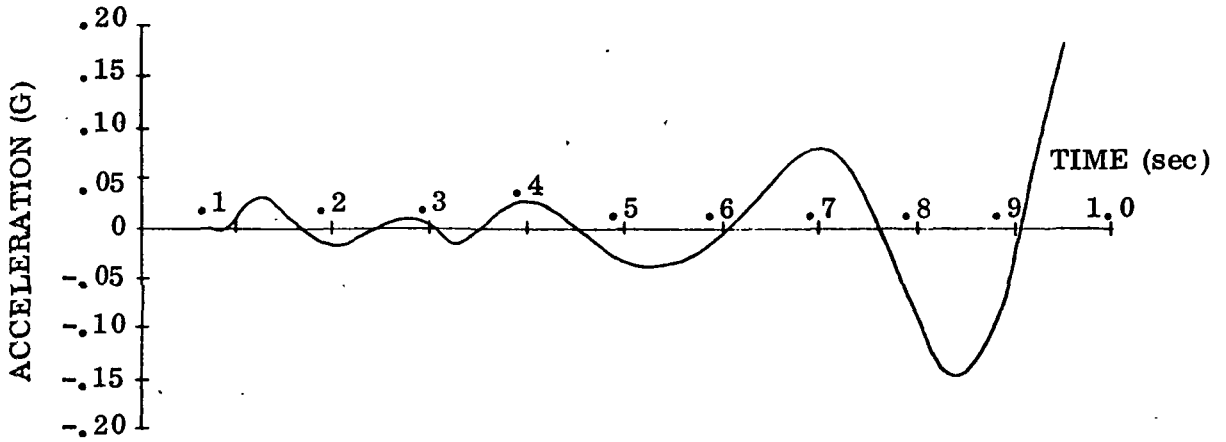

b. Rigid Body Plus 10 Elastic Modes and Autopilot

Figure 3-6. Autopilot Effects on Vehicle Response

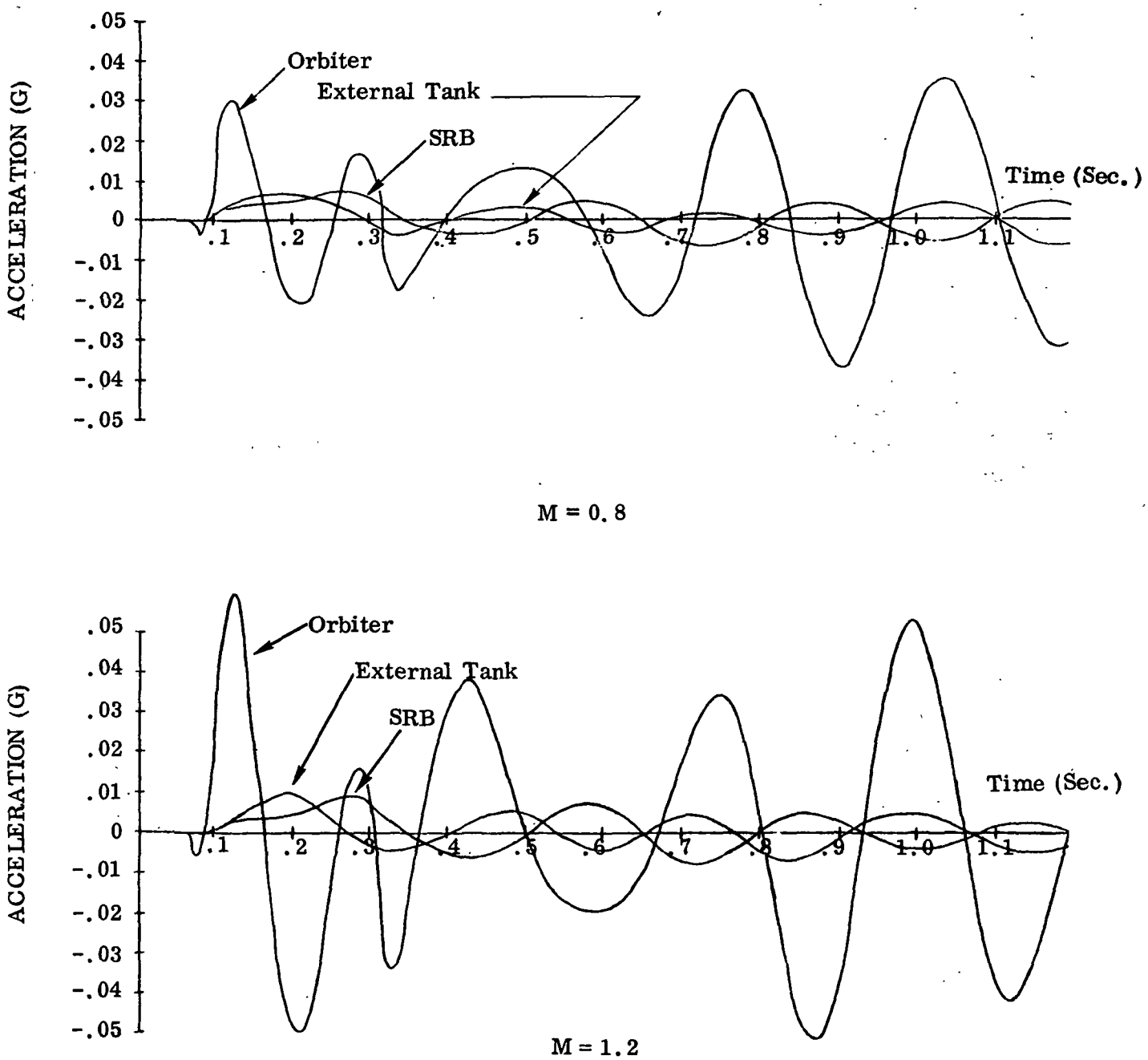

Figure 3-7. Configuration C.G. Acceleration Time Histories

The peak acceleration responses are summarized in Figures 3-8 through 3-10. As can be seen, the shortest period gust produces the maximum acceleration at the nose of each vehicle, with the Mach 1.2 response about twice the response at Mach 0.8. The acceleration over the mid- and aft portions of the vehicles is relatively insensitive to gust period. The peak acceleration at the orbiter nose for a design (9-m/s) gust is about 1.8g. Figure 2-39 of Reference 3 showed a peak acceleration on the orbiter nose at Mach 1.2 due to a 9-m/s gust would be about 1.6g for the fully reusable space shuttle configuration.

Figures 3-11 and 3-12 show the peak shear and bending moment envelopes, respectively, due to a 1-m/s, 0.22 second period, quasi-square wave gust. These are the absolute peak values and do not occur simultaneously. Due to the method used in integrating the loads to obtain shears and moments, the values shown at the aft end of the vehicles (from the aft attachments back) are incorrect.

It is interesting to compare the gust loads with those obtained in the static aeroelastic analysis. Taking the gust bending moments occuring at the stations at which the static bending moments (Figures 3-2 through 3-4) are maximum, and multiplying by 9-m/s (the design gust velocity), the following values are obtained:

		Bending Moment (10^6 N-m)	
Vehicle	Station (m)	M = 0.8	M = 1.2
ET	38	2.3 (1.08)	2.4 (1.98)
SRB	43	0.5 (0.27)	1.0 (0.36)
Orbiter	50	1.9 (0.72)	2.3 (0.96)

The values in parentheses are due to the design gust. It can be seen that gust bending moments are about half of the static values, or in other words, the maximum static bending moment must be increased by approximately 50-percent to account for the gust.

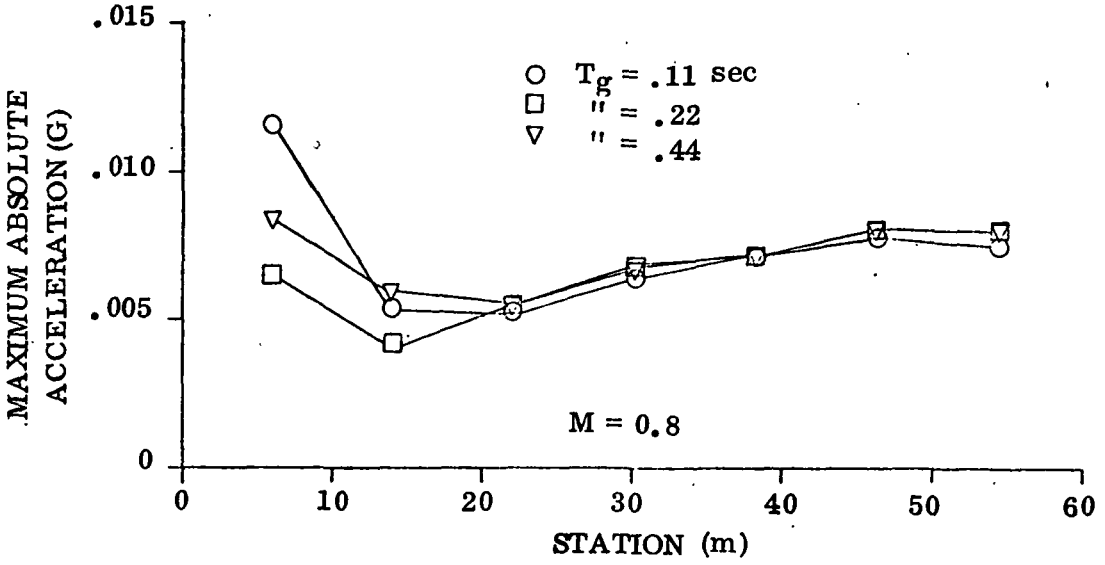

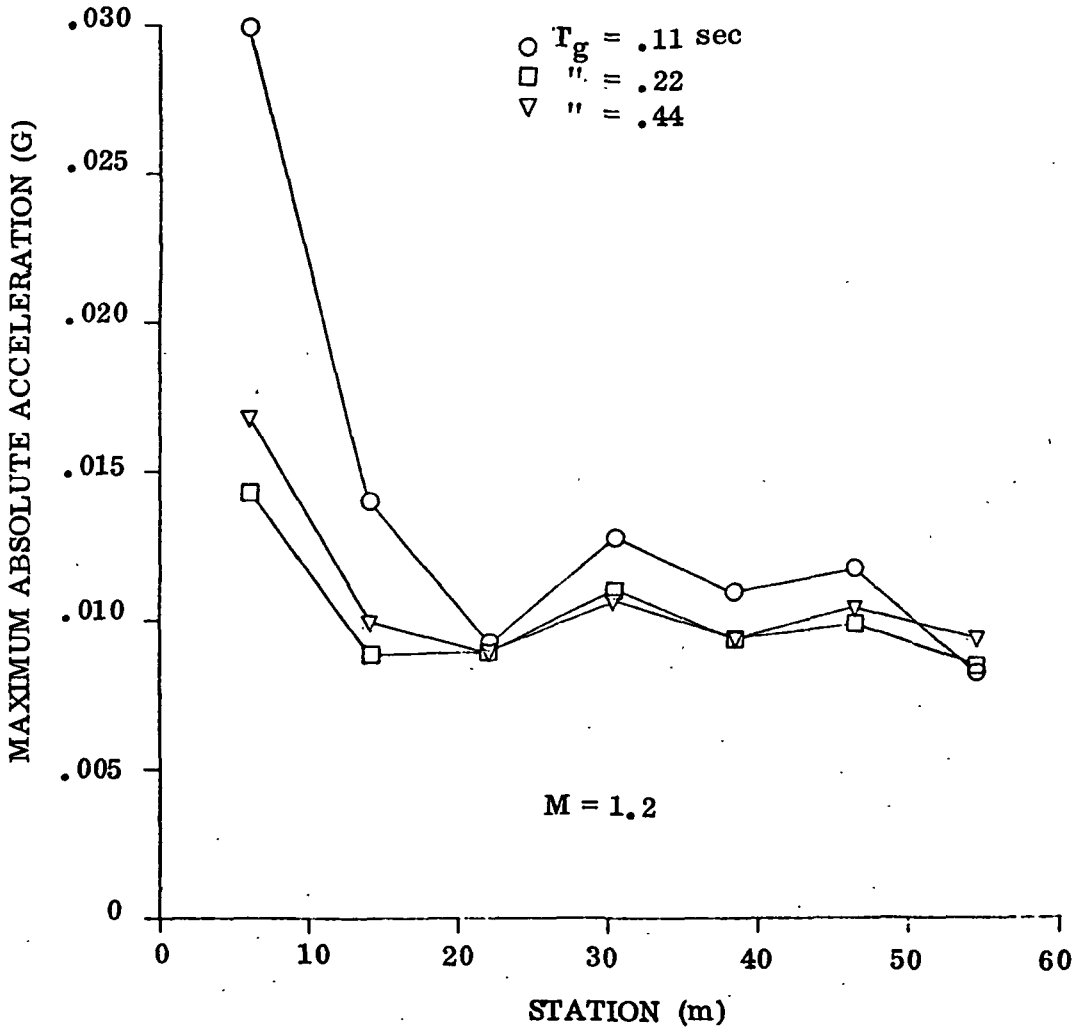

Figure 3-8. ET Maximum Accelerations Due to 1-m/s Quasi-Square Wave Gust

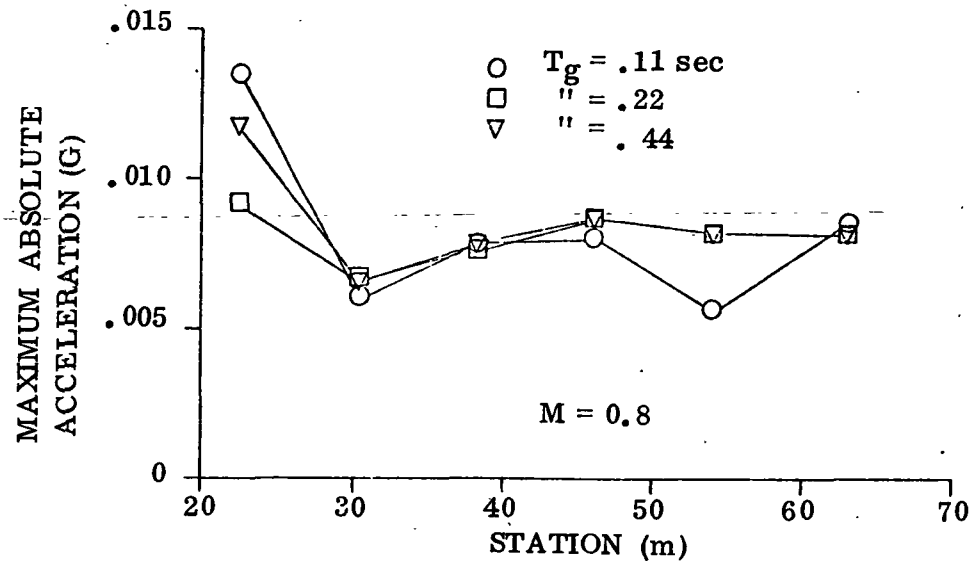

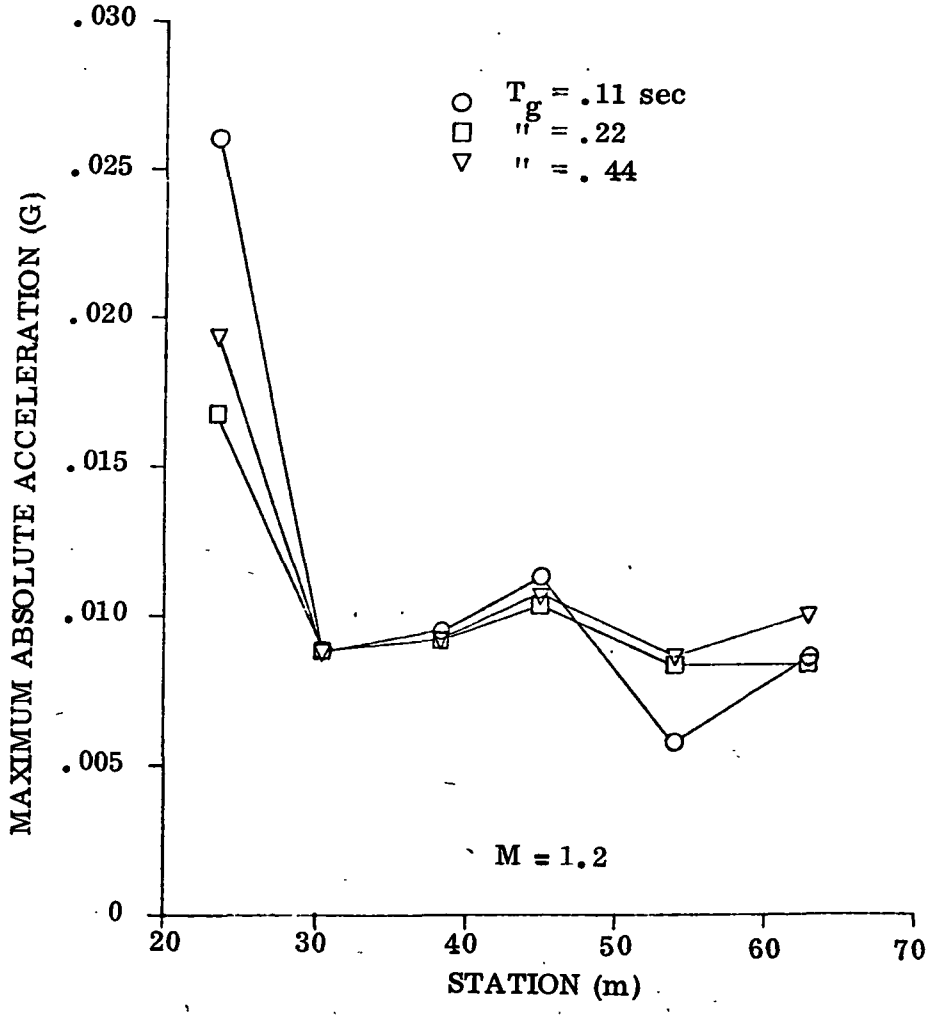

Figure 3-9. SRB Maximum Accelerations Due to 1-m/s Quasi-Square Wave Gust

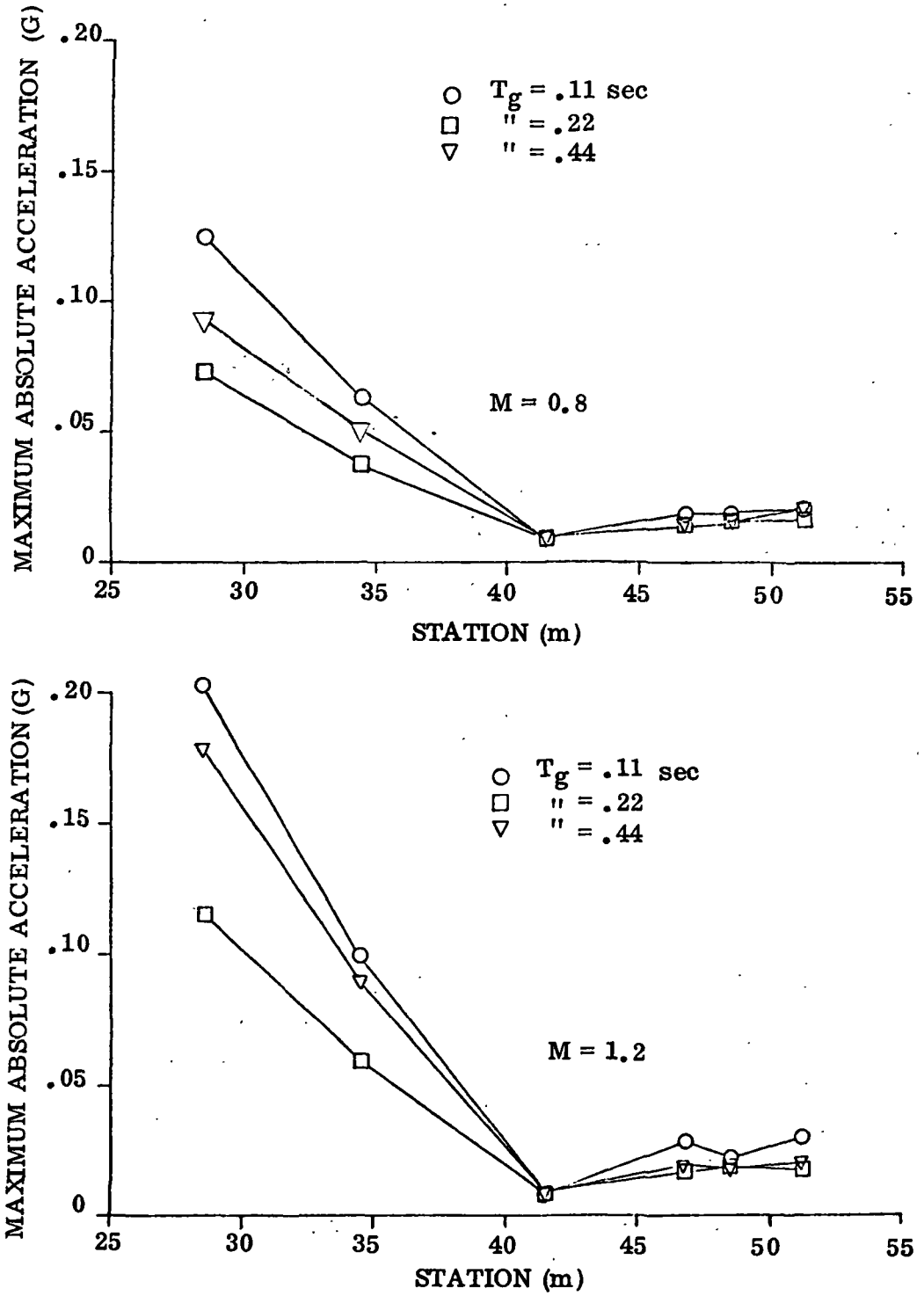

Figure 3-10. Orbiter Maximum Accelerations Due to 1-m/s Quasi-Square Wave Gust

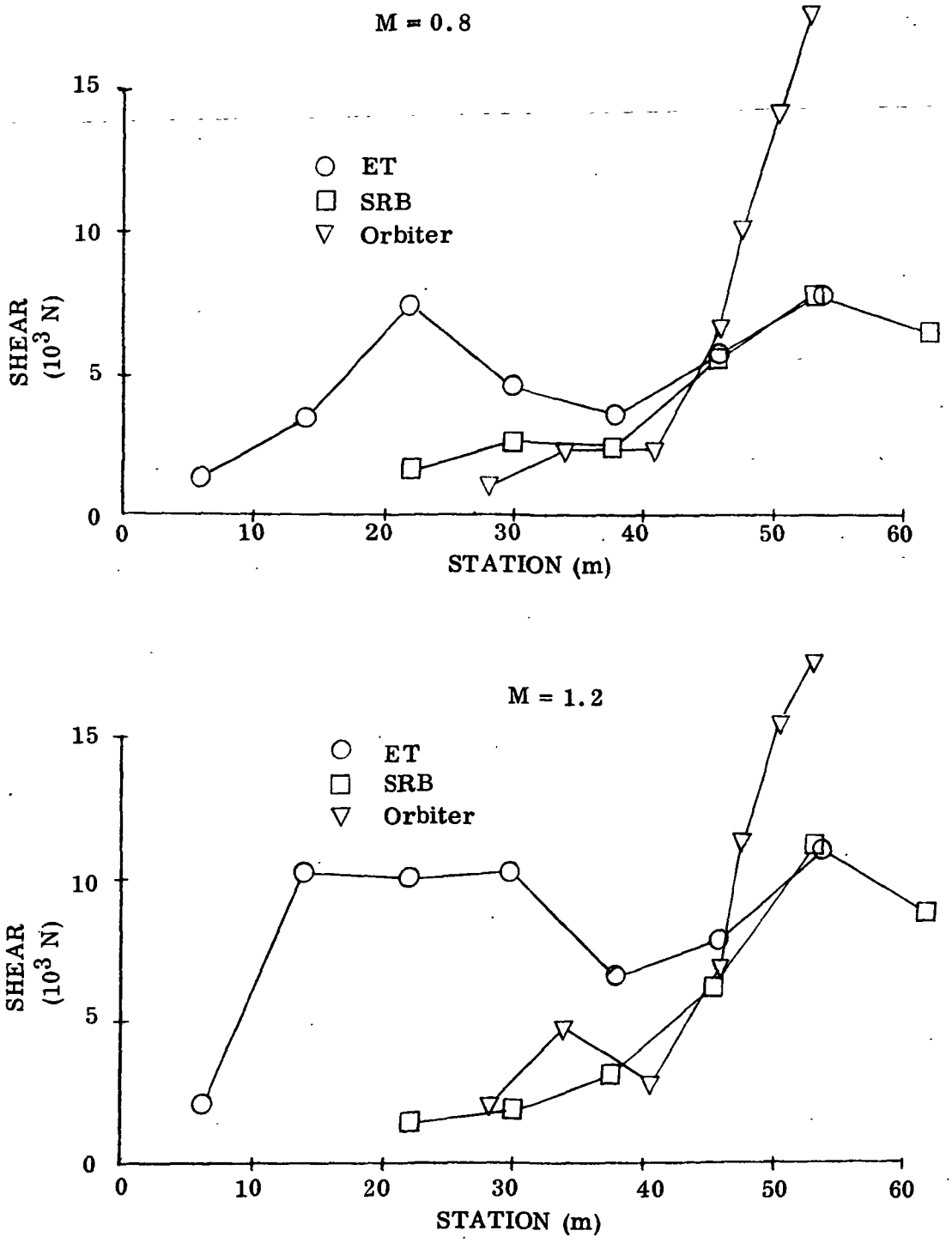

Figure 3-11. Maximum Shears Due to 1-m/s, 0.22 sec. Period, Quasi-Square Wave Gust

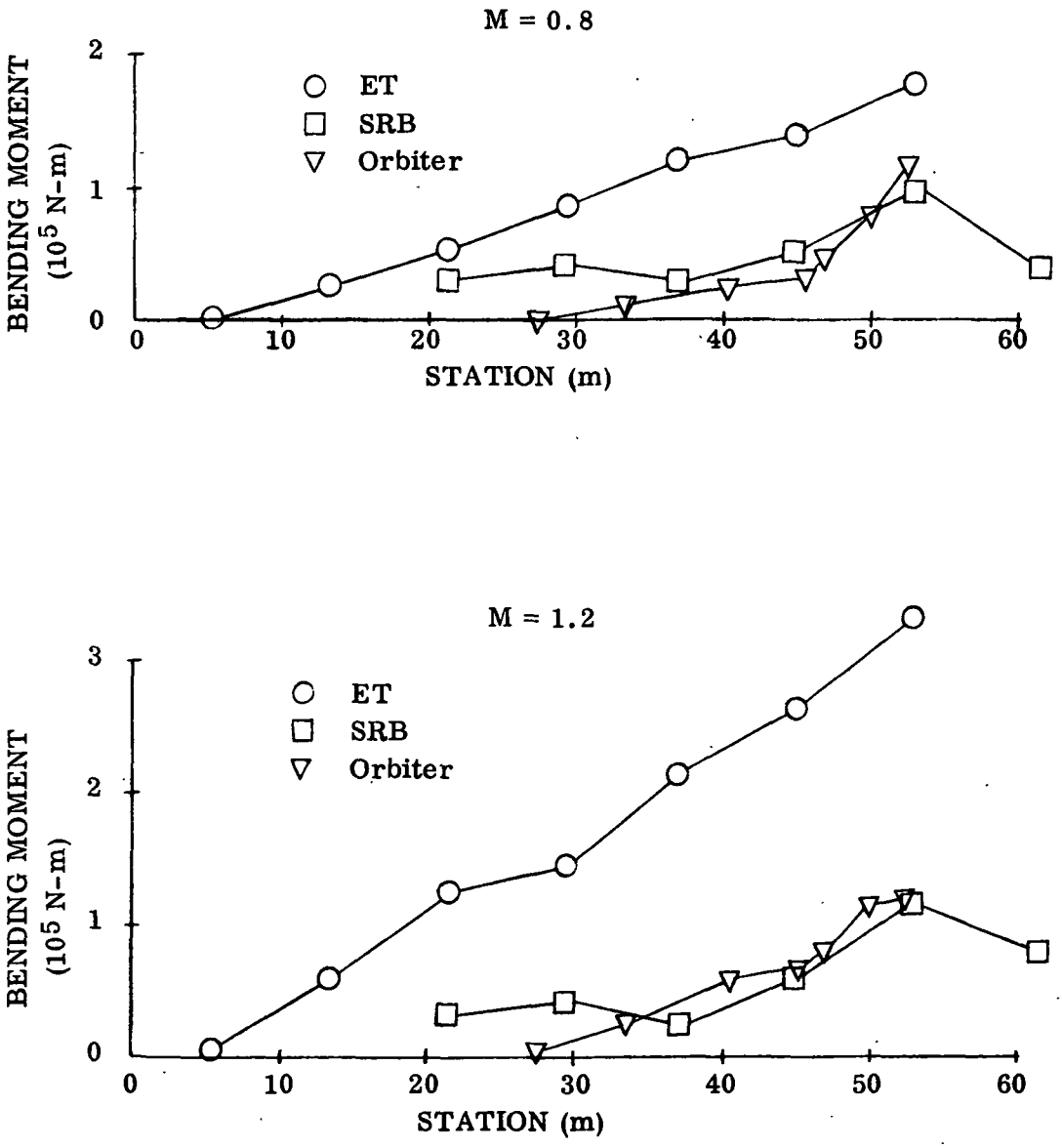

Figure 3-12. Maximum Bending Moments Due to 1-m/s, 0.22 sec. Period, Quasi-Square Wave Gust

SECTION 4

CONCLUSIONS

The simplification in going from interference to lumped aerodynamic data has been found to give adequate results for preliminary design aeroelastic analyses.

A comparison of the detailed (frequency domain) turbulence response analysis with the simplified (time domain) method indicates that the simplified approach gives good results.

Applying these simplified tools to the current space shuttle configuration has revealed that the gust loads are approximately 50-percent of the maximum static aeroelastic loads. This is a larger percentage than for conventional launch vehicles where typically, the gust loads are 20-percent of the static values at maximum αQ.

The autopilot became unstable when the ten elastic modes were included. This is not surprising since the gains were established from a rigid body analysis. When only the first elastic mode was included, the system was stable.

It was also found that at the nose of the orbiter, the design gust produced a peak acceleration of 1.8g. This compares to 1.6g reported in Reference 3 for the earlier fully reusable space shuttle configuration.

In the static aeroelastic analysis, elastic effects were found to be small (less than 3-percent).

SECTION 5

REFERENCES

1. R. G. Huntington, A Method for Determining the Response of Space Shuttle to Atmospheric Turbulence, "Volume I, Space Shuttle Turbulence Response," GDC-DDE71-002, Convair Aerospace Division of General Dynamics, 1 November 1971.

2. R. G. Huntington and R. L. Haller, A Method for Determining the Response of Space Shuttle to Atmospheric Turbulence, "Volume II, Computer Program Description and Usage Instructions," GDC-DDE71-006, Convair Aerospace Division of General Dynamics, December 1972.

3. R. G. Huntington, Space Shuttle Ascent Flight Turbulence Response, GDCA-DFM72-009, Convair Aerospace Division of General Dynamics, 15 September 1972.

4. R. G. Huntington, Space Shuttle Response to Atmospheric Turbulence, AIAA Dynamics Specialists Conference, Williamsburg, Virginia, March 19-20, 1973.

5. A. L. Odorico and V. K. Bertel, Gust Response Program No. 2466, CCD-PROG-012, Convair Aerospace Division of General Dynamics, 25 September 1964.

6. F. A. Woodward, "Analysis and Design of Wing-Body Combinations at Subsonic and Supersonic Speeds," Journal of Aircraft, Vol. V, No. 6, 1968.

7. Terrestrial Environment (Climate) Criteria Guidelines for Use in Space Vehicle Development, 1971 Revision, TM-X-64589, NASA, 10 May 1971.

8. A. L. Odorico and D. Lestico, Static Aeroelastic Program No. 3558, CCD-PROG-013, Convair Aerospace Division of General Dynamics, 17 November 1964.